

1 *Abstract*

2 Whether modeling the evolution of a discrete or continuous character, the focal trait of interest
3 does not evolve in isolation and require comparative methods that model multivariate evolution.
4 Progress along these lines has involved modeling multivariate evolution of the same class of
5 character and there are fewer options when jointly modeling traits when one character is discrete
6 and the other is continuous. Here we develop such a framework to explicitly estimate the joint
7 likelihood for discrete and continuous characters. Specifically, our model combines the
8 probability of observing the continuous character under a generalized OU process with the
9 probability of the discrete character under a hidden Markov model, linked by a shared underlying
10 regime. We use simulation studies to demonstrate that this approach, *hOUwie*, can accurately
11 evaluate parameter values across a broad set of models. We then apply our model to test whether
12 fleshy and dry fruits of Ericaceae lineages are correlated with their climatic niche evolution as
13 represented by the aridity index. Consistent with expectations, we find that dry fruits have higher
14 rates of climatic niche evolution, that the climatic niche of fleshy fruits is more conserved, and
15 dry fruits have a more humid climatic optimum.

16

17 A common theme in comparative biology is the detection of causal, or least mechanistic,
18 factors that affect the evolution of quantitative characters. Questions of how plant life habit
19 influence genome size evolution (Beaulieu et al. 2012), how substrate use alters limb length
20 evolution (Mahler et al. 2013), or how tooth morphology slowly changes in response to habitat
21 and diet (Toljagić et al. 2018) are all examples of testing whether evolutionary changes in a
22 discrete variable may have altered evolutionary trajectories of a continuously varying trait. One
23 very common phylogenetic comparative approach for these types of questions is to employ an
24 Ornstein-Uhlenbeck (OU) model, which assumes distinct regimes, described by the evolution of
25 a discrete character, are known completely *a priori* (e.g., Butler and King 2004; Hansen et al.
26 2008; Beaulieu et al. 2012), or assumes that “shifts” in regimes can be inferred directly from the
27 distribution of the continuous trait (e.g. Ingram and Mahler 2013; Uyeda and Harmon 2014;
28 Khabbazian et al. 2016). While these approaches are practical, the discrete trait is assumed the
29 driving force underlying the evolution of the continuous character. However, dependence rarely
30 flows just one way in evolution, and we suspect that as often as a discrete character causes
31 change in the continuous character, continuous characters also influence discrete character
32 evolution, or at the very minimum, can provide information about how they may be evolving in
33 tandem.

34 Progress along these lines has mostly involved acknowledging uncertainty in the
35 evolution of the discrete character by fitting models over a large set of stochastically generated
36 character mappings. That is, a large set of alternative reconstructions of the discrete character are
37 obtained completely uninformed by the continuous trait’s evolution, then the likelihood of the
38 continuous character becomes the average of the likelihoods across these maps (e.g., Revell
39 2012). The advantage of this approach is that there is an explicit model for how regimes change

40 through time, but the evolution of these regimes remains entirely independent of the continuous
41 trait, and the probability of these regimes is not explicitly considered. For example, it is possible
42 that the model that best fits the discrete data generates stochastic maps that does not provide a
43 good fit to the continuous data.

44 A promising approach was recently described for detecting adaptive codon evolution
45 (Jones et al 2020), where a set of maps obtained for a discrete phenotype under a standard
46 Markov process is optimized along with parameters associated with genotype properties, thus
47 forcing an emergent dependency between the two. Similarly, May and Moore (2020) developed
48 a joint model for discrete and continuous characters under a state-dependent Brownian motion
49 model. Their approach takes advantage of prior probabilities within a Bayesian framework to
50 accommodate variation in the “background” rate of evolution in the continuous trait (i.e., rate
51 variation across lineages that is independent of the discrete character under consideration). The
52 novel Bayesian pipeline recently developed by Tribble et al. (2021) is the first attempt that we
53 are aware of for jointly modeling discrete and continuous traits under an OU framework. Their
54 approach samples discrete stochastic mappings informed by the discrete trait along with regime
55 mappings which were informed by the continuous trait while accounting for the potential of
56 hidden variation. While a more effective test of correlation between discrete and continuous
57 characters, one drawback is that they do not explicitly account for the joint probability of the
58 discrete and continuous parameter estimates together. They assume that the combination of
59 independently estimated discrete and continuous models produces a joint estimate.

60 Here we develop and implement a framework that provides an explicitly joint estimate of
61 the likelihood for a discrete and continuous character. Specifically, our model combines the
62 probability of the continuous character given a particular regime evolving under a generalized

63 OU process, and the probability of that discrete regime painting obtained from an expanded set
64 of Markov models, integrated over many regime paintings. We demonstrate how our framework,
65 which we call *hOUwie*, can be used to test hypotheses of correlated evolution between discrete
66 and continuous characters while also accounting for hidden character states and unobserved
67 variation. Finally, we apply several *hOUwie* models to test the correlated dynamics of the mode
68 of seed dispersal and climatic niche evolution and compare our results to those that did not
69 account for the potential joint evolution of discrete and continuous variables.

70

71

Materials and Methods

72

The hOUwie model

73

74

75

76

77

Our model is composed of two processes: one describing the evolution of a discrete
character and the other describing the evolution of a continuous character. To model the
evolution of a single continuous character we use an Ornstein-Uhlenbeck (OU) model (Hansen
1997; Butler and King 2004; Hansen et al. 2008; Beaulieu et al. 2012; Ho and Ané 2014a).
Formally, the OU process is an Itô diffusion satisfying:

78

$$dX(t) = \alpha(\theta(t) - X(t)) + \sigma dB(t).$$

79

80

81

82

83

84

85

Conceptually, this model combines the stochastic evolution of a trait through time with a
deterministic component that models the tendency for a trait to evolve towards an “optimum.” In
this model, the value of a trait, $X(t)$, is pulled towards an optimum, $\theta(t)$, at a rate scaled by the
parameter α . The optimum, $\theta(t)$, is a piecewise constant on intervals and takes values in a finite
set $\{\theta_i\}$. This can represent the set of “selective regimes”, “regimes”, or Simpson’s “adaptive
zones” (Cressler et al. 2015), though it is consistent with a variety of true underlying
microevolutionary models (Hansen 2014). Additionally, random deviations are introduced by

86 Gaussian white noise $dB(t)$, which is distributed as a normal random variable with mean zero
87 and variance equal to $\sigma^2 dt$. Thus, σ^2 is a constant describing the rate of stochastic evolution
88 away from the optimum. We use the set of extensions introduced by Beaulieu et al. (2012) and
89 implemented in the R package *OUwie*, which allows for multiple primary optima $\theta(t)$ in which
90 both the pull strength (α) and the rate of stochastic evolution (σ^2) can vary across the phylogeny.
91 However, the algorithm used to calculate the likelihood described in Beaulieu et al. (2012)
92 involves a computationally costly matrix inversion procedure. Here we implement a linear-time
93 computation of the likelihood of Gaussian trait models following (Ho and Ané 2014a). To do
94 this, we first transform the phylogeny such that its variance covariance matrix, V , is 3-point
95 structured. We can write the variance covariance matrix of the untransformed phylogeny as $V =$
96 $D_u \tilde{V} D_u$, where following Beaulieu et al. (2012) and Ho and Ané (2014),

$$97 \quad \tilde{V}_{ij} = \sum_{\gamma=1}^{\kappa(i,j)} \frac{\sigma_{ij,\gamma}^2}{2\alpha_{ij,\gamma}} (e^{2\alpha_{ij,\gamma}s_{ij,\gamma}} - e^{2\alpha_{ij,\gamma}s_{ij,\gamma-1}}),$$

$$98 \quad \text{and, } D_u = e^{\sum_{\gamma=1}^{\kappa(i)} \alpha_{i,\gamma}(s_{i,\gamma} - s_{i,\gamma-1})},$$

99 where, s_γ is the distance from the root to the beginning of the selective regime (γ) for the κ
100 number of selective regimes along the path from the root to the last common ancestor of i and j ,
101 $\kappa(i, j)$, or from the root to the terminal tip i , $\kappa(i)$. Our transformed phylogeny now has a variance
102 covariance matrix \tilde{V}_{ij} and diagonal matrix D_u . We can then calculate the quadratic quantities and
103 determinant of V (Ho and Ané 2014a). The probability of our continuous trait is given by

$$104 \quad \log(P(X|D, z, \vartheta, \psi)) = n \log(2\pi) + \log(\det(V)) + \frac{P'V^{-1}P - 2P'V^{-1}Q + Q'V^{-1}Q}{2},$$

105 where n is the number of tips in the phylogeny (ψ), P is the continuous trait value of each
106 species, and Q is the expected value of each species given the continuous trait model calculated

107 following equation (11) of Beaulieu et al. (2012), D is the discrete character data, z is a particular
108 regime mapping, and ϑ are the parameters of the *hOUwie* model.

109 Next, we describe the calculation of the probability of the underlying regime structure, γ ,
110 that is the joint probability of discrete characters (D) and stochastic mapping (z). This calculation
111 is analogous to the pathway likelihood of Steel and Penny (2000). To calculate the probability of
112 discrete characters (D) and stochastic mapping (z) we use an approximation. Our approximation
113 relies on a finite number of degree-2 internodes and uses the standard Chapman-Kolmogorov
114 equation to calculate the probabilities of beginning in a particular state i and ending in state j
115 (Pagel 1994) and is identical to a joint probability of a set of state reconstructions (Yang 2006).
116 As the number of internodes increase, the amount of time between nodes decreases and the
117 approximation improves (Rao and Teh 2013). The joint probability of a regime structure and the
118 discrete character i

$$119 \quad P(D, z|Q, \psi) = P(x_0|Q, \psi) \prod_{\ell=1}^{n-1} P(z_\ell|Q, T_\ell),$$

120 where \mathbf{Q} the instantaneous rate matrix ($\mathbf{Q} \in \vartheta$), ψ is the phylogeny, $P(x_0|\mathbf{Q}, \psi)$ is the root state
121 probability (Pagel 1994; Yang 2006; Maddison et al. 2007), n is the number of external nodes
122 (tips), internal nodes, and internodes (degree-2 nodes) summed, ℓ indicates a particular branch,
123 $P(z_\ell|\mathbf{Q}, T_\ell) = e^{\mathbf{Q}T_\ell} \mathbb{1}_\gamma$, where $\mathbb{1}_\gamma$ is an indicator function which ensures that we only use the
124 probability of states indicated by the specific the regime mapping instead of summing over all
125 possible state combinations. The continuous character probability requires the discrete state(s) to
126 be defined along the entire branch, thus we place transitions halfway between any two nodes.

127 For each set of parameters evaluated during the maximum likelihood search, a set of
128 possible mappings of discrete states and continuous regimes are generated to evaluate the

129 discrete and continuous likelihoods. Ideally, we would calculate the likelihood by summing
130 across all possible reconstructions (note that we want the sum across the reconstructions, not the
131 single reconstruction with highest likelihood). The number of such reconstructions is very large,
132 $n_{\text{states}}^{(2 * \text{number of taxa} - 2)(1 + \text{number of degree two internodes per edge})}$,
133 which is particularly daunting as the sum must be calculated anew for every unique examined set
134 of parameter values as part of search. We found in early work where we did look at this
135 exhaustively that a few mappings made up the vast majority of the total likelihood, so we set up
136 the analysis to focus on calculating total likelihood given the highest probability mappings.

137 To do this, we first approximate the conditional state probabilities at nodes. The
138 conditional state probability, unlike the more common marginal reconstruction or joint state
139 reconstruction (Pupko et al. 2000; Felsenstein 2004; Yang 2006), calculates the probability that a
140 node has a particular state value conditioned only on the observations of its descendants. For a
141 particular focal node, we calculate the probability of the observing all pairwise descendant values
142 given the OU model parameters, integrated over all possible rootward node states, and observed
143 tipward discrete states (Fig. 1). Although this is only an approximation of the conditional state
144 probabilities, it proves to be an essential improvement over the typical procedure of sampling
145 many stochastic maps based solely on the discrete process. Next, the conditional probabilities of
146 states at nodes are sampled starting with the root. Once the root is sampled, descendent states are
147 sampled based on both the conditional ancestral values and the sampled ancestral state. This is
148 achieved by multiplying the conditional probability of the node states by the probability of
149 starting in the sampled rootward ancestral value and ending in any of the tipward states (the latter
150 is calculated using familiar matrix exponentiation methods; e.g., Pagel 1994). Finally, under
151 usual stochastic mapping procedures we would use rejection sampling (Nielsen 2002; Rao and

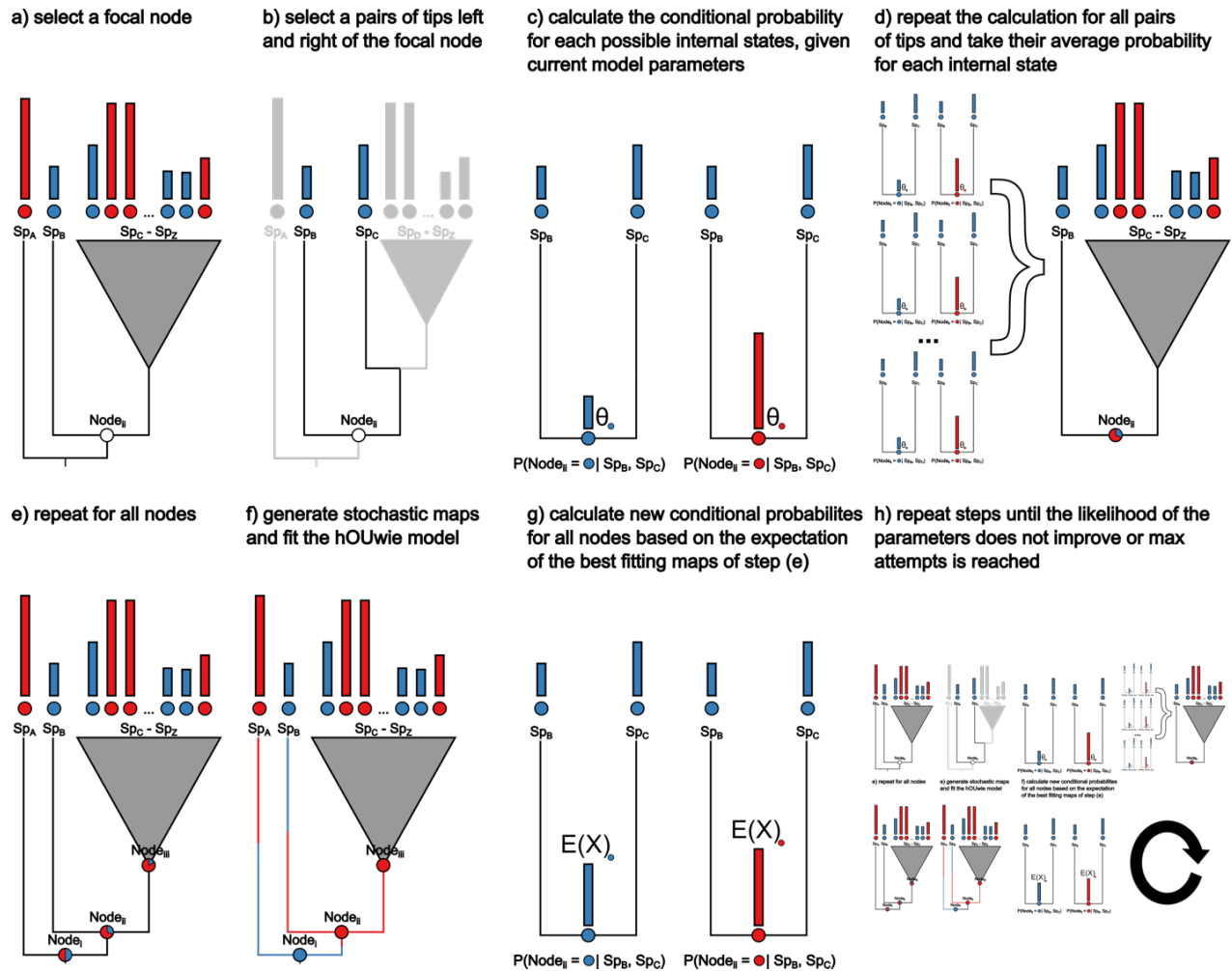


Figure 1. A visual representation of the algorithm underlying the calculation of conditional node probabilities and the adaptive sampling procedure. The goal of the procedure is to produce underlying regime paintings well suited to both the discrete and continuous character. a) select the focal node for which we will be calculating the joint conditional probabilities of the discrete and continuous characters. b) on each side of the node we select a pair of tips. c) the conditional probability of the observed discrete and continuous character is calculated for each discrete regime state with an ancestral continuous value equal to θ of that regime state. d) the conditional probability of the focal node is calculated as the average probability of each regime state for all pairs of observed tips. e) the conditional probabilities are calculated for all internal nodes. This can be turned off within hOUwie by setting the `sample_nodes` argument to false. f) A stochastic map is generating using forward simulation rejection sampling. g) adaptive sampling uses the highest joint probability of previously generated underlying regimes to generate a set of ancestral continuous character values. This differs from previous ancestral values because instead of assuming the value θ for each regime state, it calculates the expected value given the root state and regime mapping for that particular node. h) we repeat steps d) through g) until the joint likelihood of the set of underlying regimes does not improve.

153 Teh 2013) to simulate a path between the sampled rootward and tipward nodes. However, for
154 increased computational efficiency, we opt to place transitions at pre-defined internodes. After
155 nodes and internodes are sampled in step two, mappings are evaluated to ensure consistency with
156 the discrete model (i.e., impossible transitions do not occur) and branches are painted based on
157 the sampled nodes with transitions occurring half-way between nodes (and remember that a
158 single edge may have multiple internodes placed on it).

159 Our function for the joint probability of a continuous and a discrete character is,

$$160 \quad P(X, D | \vartheta, \psi) = \sum_z P(X | D, z, \vartheta, \psi) P(D, z | \vartheta, \psi),$$

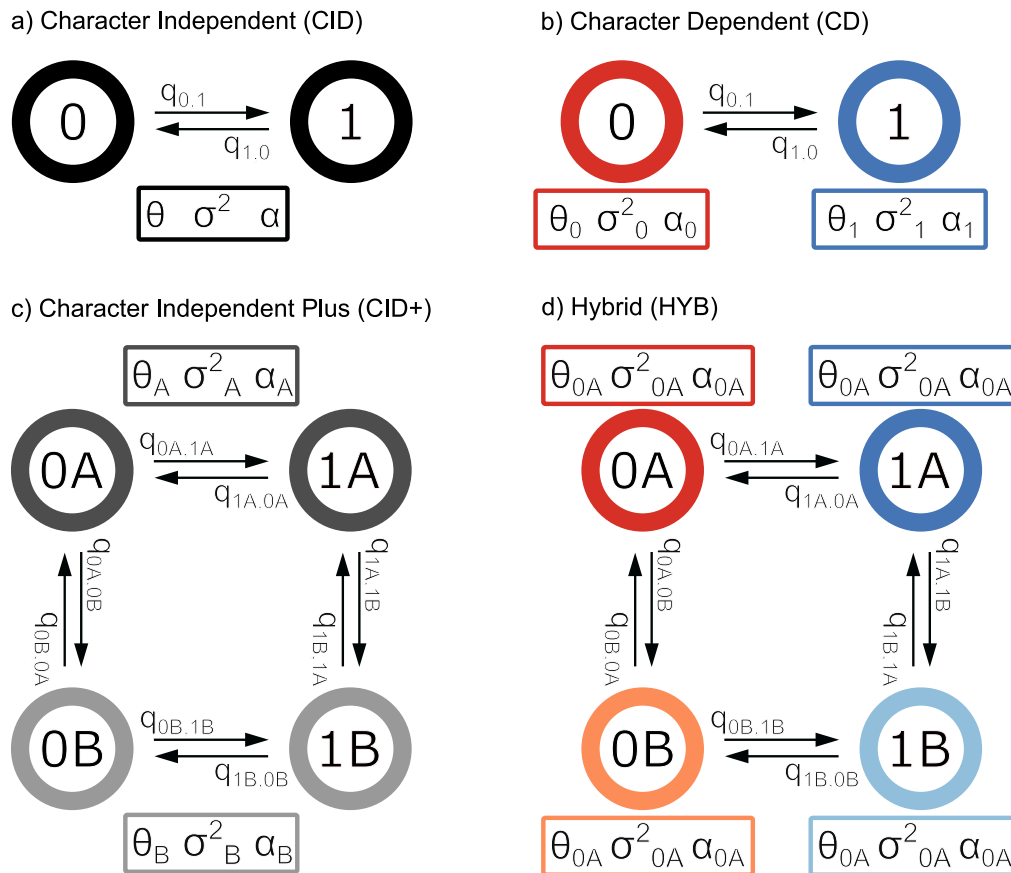
161 where summing over all generated maps (z), $P(X | D, z, \vartheta, \psi)$ is the probability of the continuous
162 character (X) given the discrete character data (D), mapping (z), hOUwie parameters (ϑ), and
163 phylogeny (ψ). $P(D, z | \vartheta, \psi)$ is the joint probability of the discrete character data (D) and
164 stochastic mapping (z) given the hOUwie parameters (ϑ) and phylogeny (ψ).

165

166 *The hOUwie model space*

167 Our simulation studies examined 22 possible hOUwie model structures for a binary
168 discrete character, although the possible number of models is significantly higher because any
169 number of discrete characters and states can be modeled together. For the discrete component of
170 the model, we assumed that transitions between the observed characters were equal. We
171 constrained transitions between hidden states to be the same for observed states, but this
172 constraint can be relaxed if desired. The continuous model structures allowable in hOUwie are a
173 generalized form of those allowed in OUwie and now include models in which only α varies
174 (OUA), only σ^2 varies (OUV), and combinations of an OU and BM process (OUBM1 and
175 OUBMV). We note that the OUBM1 model within hOUwie differs from The Ornstein–

176 Uhlenbeck Brownian-motion (OUBM) model presented in Hansen et al. (2008) and Bartoszek et
 177 al. (2012) since the latter models are of multiple continuous characters, rather than different
 178 processes describing the same continuous character.



179

Figure 2. A state-transition diagram describing the model classes allowable in hOUwie. Each panel is comprised of observed discrete states 0 and 1 with possible hidden states A and B. Transitions between states are described with the q parameter. Continuous model parameters appear in a box below the states they describe, and their association is displayed with a subscript specific to that state. a) A simple character independent model in which the two observed states do not influence the continuous character which will have the same θ, σ^2, α throughout the phylogeny. b) A character dependent model in which the continuous character depends on the discrete character by virtue of θ, σ^2, α being associated with a particular observed discrete state. c) A character independent model with rate heterogeneity. The two observed states (0 and 1) are not directly linked to the continuous character. However, the continuous character is still allowed to have multiple θ, σ^2, α describing its evolution, but these parameters are associated with hidden states A and B. d) A hybrid model in which each combined observed and hidden state is allowed to have its own θ, σ^2, α . Under this model, the continuous character is linked to both character dependent differences (parameters associated with 0 and 1) and character independent differences (A and B). Though this diagram shows a binary observed and hidden character, either can have more states (up to 26 states for each in theory, though few datasets will have enough power to estimate the necessary number of parameters).

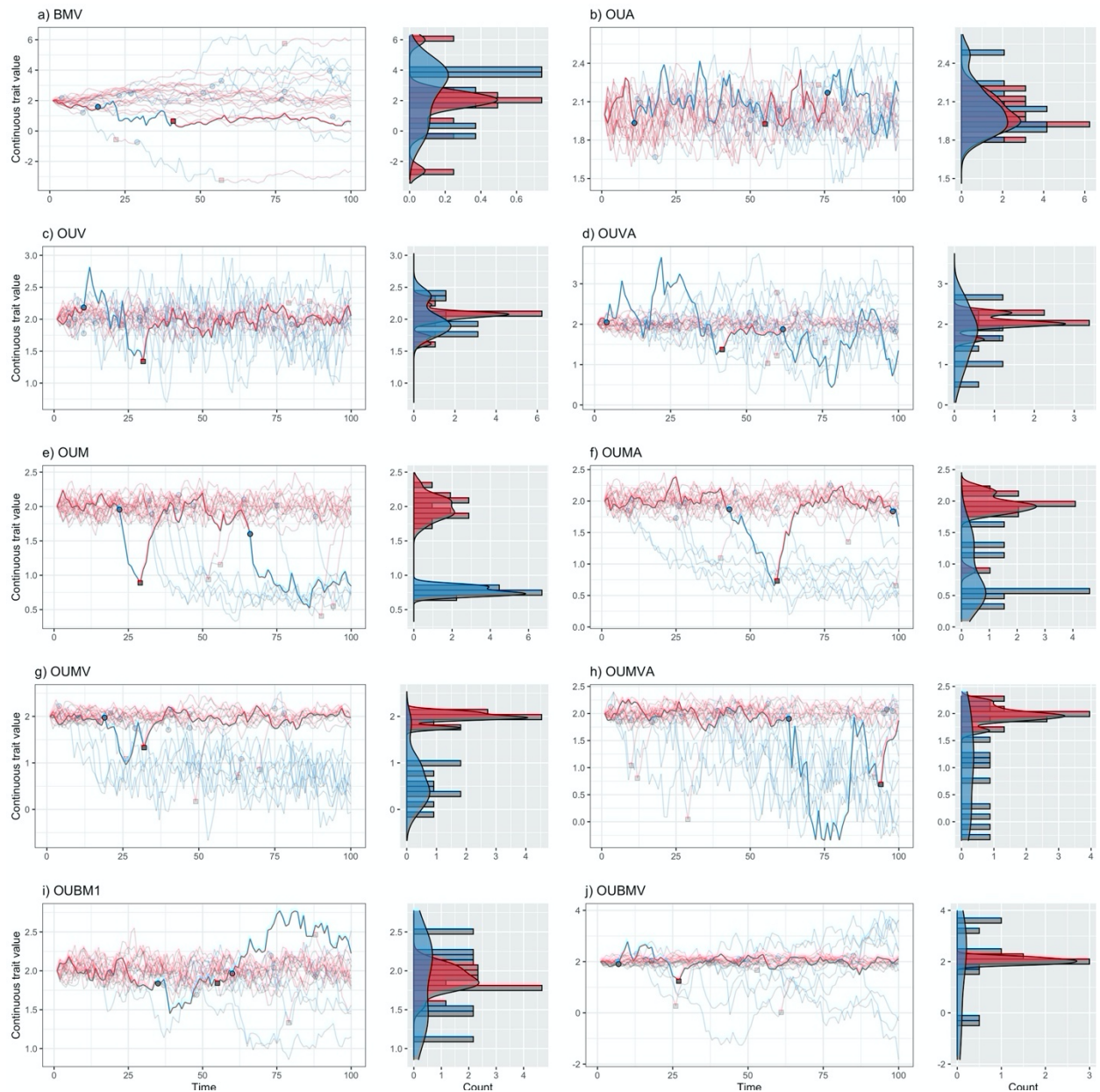


Figure 3. A visual representation of binary discrete character $hOUwie$ model types. Discrete time forward simulations are conducted starting in the red state and the distribution of the continuous character is plotted on the right as a histogram and density plot. Each line represents a continuous character value at some time. Transitions occur at colored points and each line is colored by the current discrete state. 100 time-steps are simulated with the same parameters as our simulation study ($q_{ij} = 0.1$, $\alpha_1 = 3$, $\alpha_2 = 1.5$, $\sigma_1^2 = 0.35$, $\sigma_2^2 = 1$, $\theta_1 = 2$, and $\theta_2 = 0.75$). The highlighted line was randomly chosen from the set in which at least one discrete state transition occurred.

203 models to assess parameter estimation accuracy and model selection power. Although this

204 represents a small subset of the potentially vast parameter space available to OU models, the

205 behavior of these models has been thoroughly characterized and thus we chose parameters within
206 the range of typical identifiability (Beaulieu et al. 2012; Ho and Ané 2014a; Cressler et al. 2015).
207 Additionally, because *hOUwie* uses a variable number of mappings, we evaluate changing the
208 number of stochastic maps. We fit each model using 25, 100, and 250 stochastic mappings per
209 likelihood evaluation. Each dataset was evaluated using the true generating model, a BM1, an
210 OU1, and either the character-dependent or character-independent counterpart to the generating
211 model. For example, if the data were simulated under a character-dependent OUM model where
212 the value of θ_1 and θ_2 depend on the observed character, a character-independent OUM model
213 would also be fit as part of the model set. Under the CID+ OUM model, a variable θ is still
214 allowed, but it is unlinked to the focal character and thus should provide a more reliable
215 character independent null hypothesis than BM1 or OU1 (Beaulieu and O’Meara 2016; Uyeda et
216 al. 2018; May and Moore 2020; Boyko and Beaulieu 2022).

217

218 *The impact of climatic variables on seed dispersal*

219 For sedentary organisms, such as plants, dispersal is mainly limited to a brief stage of
220 their life cycle and mediated mainly through the movement of seeds (Levin et al. 2003).

221 Generally, the expectation is that seeds dispersed by frugivores are going to be dispersed to
222 environments more like their parents’ environment, whereas abiotically dispersed seeds are
223 likely to be more erratic in their dispersal patterns (Schupp 1993; Westoby et al. 1996).

224 Furthermore, it has been proposed that adaptations for frugivorous dispersal is linked to tropical
225 and subtropical biomes, because in these warmer and wetter habitats, large trees create shady
226 environments where competition for light is more important. A shadier habitat then imposes a
227 selective pressure for larger seeds because more nutrients are needed for germination and initial

228 survival (Foster and Janson 1985). However, the evolution of larger seeds comes with a tradeoff
229 as they have a significantly lower dispersal potential (Howe and Smallwood 1982). Thus, we
230 might expect that the climatic variables of a habitat influence the probability of transitioning
231 between abiotic and biotic modes of dispersal, with transition rates from abiotic to biotic being
232 greater in less arid environments.

233 Here we use dry or fleshy fruit morphology as a proxy for abiotic or biotic seed dispersal
234 (Lorts et al. 2008) to evaluate three predictions outlined in Vasconcelos et al. (2021), but
235 specifically measuring the aridity index. First, we expect that the climatic optima for fleshy fruits
236 will be more humid compared to dry fruits ($\theta_{\text{dry}} < \theta_{\text{fleshy}}$). Second, we expect that dry fruits
237 will have faster rates of climatic niche evolution ($\sigma_{\text{dry}}^2 > \sigma_{\text{fleshy}}^2$). Finally, we expect that the
238 climatic niches of fleshy fruits will be more conserved through time ($\alpha_{\text{dry}} < \alpha_{\text{fleshy}}$). We apply
239 several *hOUwie* models to test these hypotheses and compare our results to those discussed in
240 Vasconcelos et al. (2021). We expect that any differences found between this study and
241 Vasconcelos et al. (2021) are because we can explicitly account for the joint probability of the
242 discrete and continuous characters. We focus our attention on Ericaceae specifically because
243 Vasconcelos et al. (2021) found two counter-intuitive results. Namely, they found that the
244 phenotypic optima of dry fruits were more humid than fleshy fruited lineages, and that the rate of
245 climatic evolution was greater in fleshy fruits than dry fruits.

246 We included 25 *hOUwie* models within our model set: 2 CID, 10 CD, 10 CID+, and 3
247 HYB. *Gaultheria* is technically a dry-fruited genus within Ericaceae but has a persistent fleshy
248 calyx that attracts frugivores (Stevens et al. 2004). However, since we are interested in the
249 association between dispersal and fruit type, we code this as fleshy fruited within our dataset.
250 Models are evaluated using the sample size corrected Akaike Information Criterion (AICc) and

251 model averaging is conducted when discussing how our results relate to our hypotheses
252 (Burnham and Anderson 2002). Measurement error is included for each model fit as within
253 species variance (the sample-sized weighted average of the individual species variances
254 following Labra et al. (2009) and Vasconcelos et al. (2021)). We evaluate then model averaged
255 parameter estimates of θ , σ^2 , and α for fleshy and dry fruited lineages, as they relate to our
256 hypotheses and compare our results to Vasconcelos et al. (2021). Finally, we conduct a
257 parametric bootstrap of 100 simulated datasets to evaluate the standard error of our model
258 averaged parameter estimates.

259

260

Results

261

Simulation study

262

263

264

265

266

267

268

269

270

271

272

273

For character-independent (CID) models, our heuristic adaptive sampling algorithm, which uses information from the discrete and continuous characters to guess at mappings, consistently produced more probable mappings than using purely discrete mappings for all models examined. On average, adaptive sampling produced mappings which were roughly 38 log likelihood units better than purely discrete sampling when examining joint probabilities. This was driven primarily by the improved continuous probabilities which were on average 38.4 log likelihood units better. In contrast, the discrete probability of each mapping was similar with discrete-only simulations producing maps that were on average 0.39 log likelihood units better (Table 1; Fig. S1). For character-dependent models, the difference was negligible (not shown). This is because when the discrete and continuous character are strongly linked, discrete-only mappings will match the continuous character's distribution quite well.

274 **Table 1.** A comparison of the effectiveness of the adaptive sampling procedure and standard
 275 discrete only sampling of maps. Regardless of the sampling procedure, all probabilities are
 276 calculated in the same way and so any differences in probabilities reflects each procedure's
 277 ability to generate appropriate mappings. 50 regime mappings are used to calculate the likelihood
 278 of the parameters. A higher \log_e likelihood is better (that is, -16.43 is better than -16.48; 10.54 is
 279 better than 9.19) For each model type, data are simulated following our methods with $q_{ij} =$
 280 $0.1, \alpha_1 = 3, \alpha_2 = 1.5, \sigma_1^2 = 0.35, \sigma_2^2 = 1, \theta_1 = 2,$ and $\theta_2 = 0.75$. The generating parameters are
 281 used to evaluate probability of each dataset and thus the probabilities represented here are not
 282 necessarily the same as those derived from the MLE. Generally, adaptive sampling improves the
 283 joint estimate by improving the probability of the continuous character and is most effective for
 284 variable θ models. As expected, discrete only sampling produces regime paintings which better
 285 reflect the discrete character than adaptive sampling, but the difference is minor.

Model class	Model type	Sampling procedure	Discrete marginal \log_e likelihood	Continuous marginal \log_e likelihood	Joint \log_e likelihood
CID+	BMV	adaptive sampling	-16.48	10.54	-10.59
		discrete only	-16.43	9.19	-10.59
	OUA	adaptive sampling	-15.46	44.34	25.14
		discrete only	-15.53	43.11	24.96
	OUV	adaptive sampling	-30.89	47.86	12.17
		discrete only	-30.14	46.00	12.11
	OUVA	adaptive sampling	-11.88	36.91	21.14
		discrete only	-11.17	36.27	21.08
	OUM	adaptive sampling	-11.94	57.57	39.08
		discrete only	-11.19	53.56	32.21
	OUMA	adaptive sampling	-9.94	35.01	17.39
		discrete only	-9.38	2.19	-20.48
	OUMV	adaptive sampling	-19.96	20.77	-15.64
		discrete only	-14.76	-2.92	-25.83
	OUMVA	adaptive sampling	-13.91	25.47	7.48
		discrete only	-13.23	26.36	4.48
	OUBM1	adaptive sampling	-14.26	42.20	24.39
		discrete only	-14.88	40.89	24.22
	OUBMV	adaptive sampling	-19.17	49.10	18.84
		discrete only	-19.01	33.45	7.71

286

287

288

289

290

291 **Table 2.** The average accuracy of *hOUwie* parameter estimates across several model classes and
 292 types as measured by root-mean-square error (RMSE). RMSE is calculated for each model type
 293 by taking the square root of the mean squared error (MSE), where MSE is the average squared
 294 difference between the MLE and the simulating parameters. Data is generated with $q_{ij} =$
 295 $0.1, \alpha_1 = 3, \alpha_2 = 1.5, \sigma_1^2 = 0.35, \sigma_2^2 = 1, \theta_1 = 2,$ and $\theta_2 = 0.75,$ and for phylogenies with 25,
 296 100, and 250 taxa. Finally, model fits use either 25, 100, or 250 stochastic maps per likelihood
 297 iteration. The table shown here calculates RMSE integrating over all phylogenetic tree sizes and
 298 number of stochastic maps (n=8217). Dashes indicate a parameter that is not estimated for a
 299 given model type. Generally, character independent (CID+) models had higher errors than
 300 character dependent (CD) models. The greatest errors occurred when estimating alpha in variable
 301 alpha models for both CD and CID+ model classes. Estimates of the optimum and transition
 302 rates generally had the lowest errors.

Model class	Model type	RMSE q	RMSE α_1	RMSE α_2	RMSE σ_1^2	RMSE σ_2^2	RMSE θ_1	RMSE θ_2
CD	BMV	0.12	-	-	0.10	0.28	0.22	-
	OUV	0.11	1.27	-	0.15	0.33	0.05	-
	OUA	0.12	1.55	1.63	0.11	-	0.06	-
	OUM	0.13	1.49	-	0.10	-	0.07	0.13
	OUVA	0.09	1.44	1.11	0.14	0.98	0.06	-
	OUMV	0.16	1.82	-	0.16	0.32	0.07	0.17
	OUMA	0.15	2.11	2.48	0.28	-	0.12	0.50
	OUMVA	0.18	1.62	1.12	0.12	1.07	0.76	1.06
	OUBM1	0.1	2.64	-	0.08	-	0.08	-
	OUBMV	0.09	2.29	-	0.13	2.37	0.08	-
CID+	BMV	0.05	-	-	0.27	10.11	0.24	-
	OUV	0.04	1.13	-	0.32	1.83	0.05	-
	OUA	0.05	2.93	1.34	0.33	-	0.07	-
	OUM	0.09	2.53	-	0.15	-	0.44	0.20
	OUVA	0.05	1.26	1.11	0.27	13.44	0.07	-
	OUMV	0.1	2.50	-	0.16	2.12	1.30	0.68
	OUMA	0.05	8.28	1.27	0.23	-	5.88	0.8
	OUMVA	0.07	5.54	1.24	0.20	9.37	8.76	1.35
	OUBM1	0.05	3.33	-	0.32	-	0.14	-
	OUBMV	0.05	3.50	-	0.27	8.79	0.14	-

303
 304 Most character-dependent models (CD) had lower overall deviations from the generating
 305 model across all model types. The RMSE was largest for alpha at 1.76 and 1.65 (if variable
 306 alpha) and errors were generally higher for more complex models. All other parameters had
 307 relatively similar RMSE, ranging from 0.1 for discrete the rate to 0.75 for σ_2^2 . The BMV (BM
 308 with variable σ), OUV (OU with variable σ), OUA (OU with variable α), and OUM (OU with

309 variable θ) models generally had the lowest errors, but there were some biases present (Table 2).
310 Most notably, alpha was biased upwards for OUM and OUV models and under variable alpha
311 models (OUA, OUMA, OUVA, OUMVA), the difference between the alpha estimates tended to
312 be larger than the generating parameter difference. The more complex models had larger error
313 variances but showed similar biases as the simple models. Finally, OUBM models showed a
314 significantly downward biased α , suggesting BM like processes (Fig. S2).

315 Character-independent models with rate heterogeneity models generally performed well
316 in terms of parameter estimates, but as expected, due to their inherent uncertainty, CID+ models
317 had larger errors than CD models. The largest error was estimates of σ_2^2 which had an RMSE of
318 8.5, although the median error value was only 0.03, suggesting that the large RMSE is driven by
319 a long rightward tail of the estimates. Like CD models, α_1 and α_2 consistently showed the
320 largest RMSE at 3.6 and 1.2. In general, α was underestimated with medians of -0.4 and -1.4
321 below the simulating values of 3 and 1.5. This means that models for CID+ models tended to be
322 more BM like even under an OU generated data (Fig. S2). Increasing the number of taxa
323 examined improved both CD and CID+ performance. The RMSE for α was nearly cut in half
324 between when moving from 25 tips to 250 tips from 5.2 to 2.8 under CID+ models (Table 3).
325 Nonetheless, some parameters continued to be estimated poorly, such as σ_2^2 . Interestingly,
326 increasing the number of stochastic maps improved CID+ performance, but did not substantially
327 improve estimation under CD models (Fig. S2c).

328

329

330

331 **Table 3.** Average AIC weight as the number of taxa increases for each model class. Gray cells
 332 indicate the AIC weight of the generating model class. In general, as the number of taxa
 333 increases the average support for the generating model class increases.

Generating model class	nTaxa	AICwt BM1	AICwt OU1	AICwt CD	AICwt CID+
CD	25	0.12	0.22	0.51	0.15
	100	0.06	0.22	0.70	0.02
	250	0.02	0.14	0.82	0.02
CID+	25	0.28	0.35	0.24	0.14
	100	0.21	0.4	0.23	0.15
	250	0.11	0.34	0.32	0.22

334
 335 Generally, evidence of CD when it was the generating model was consistent across all
 336 model types. The lowest support for the OUA and OUBM1 models at an average AICwt of 0.31
 337 and 0.13. For complex models, such as OUMVA, model support for was 0.81 and highest for
 338 OUMV at 0.97. CID+ models fared worse in terms of generating consistent support even when
 339 they were the generating model. Models which were difficult to estimate under character
 340 dependence were difficult to find consistent support for under character independence. The most
 341 extreme case was OUA model for which CID+ model was never chosen as the best supported
 342 model. However, models which performed well for CD tended to perform well under CID+. For
 343 example, OUM models garnered consistent support when with an average AICwt of 0.733
 344 (Table S1; Fig. S3). While the best model under AICc need not be the generating model (for
 345 example, for a small dataset a simpler model may lose less information than the generating
 346 model) given the size of the simulated trees and distinctness of the models we expect the
 347 generating model to generally be the best.

348 For both CD and CID+ models, support improved when increasing the number of tips
 349 analyzed. Support for a CD model when CD was the generating model increased from $w_{CD} =$
 350 0.5 to $w_{CD} = 0.67$ to $w_{CD} = 0.79$ for 25, 100, 250 tips and support for a CID+ model when it
 351 was the generating model increased from $w_{CID+} = 0.11$ to $w_{CID+} = 0.15$ to $w_{CID+} = 0.22$

352 (Table 3). Similarly, increasing the number of regime maps generally improved the fit, but not as
353 much as increasing the number of tips. We found that the false evidence of correlation (as
354 measured by the average AICwt of a character-dependent model when character-independence
355 was the generating model) was generally not an issue for variable θ models (OUM*). Variable θ
356 models had average AICwts for false character-dependence ranging from 0.03 to 0.23 and for
357 none of our simulations models was a CD model best supported. Under a simple OUM model,
358 CID+ models helped correct any potential bias with an average AICwt of 0.68. However, false
359 evidence of correlation was an issue for variable σ_i^2 and α_i models. False support for CD as
360 measured by AIC weight ranged from 0.34 to 0.44 when θ was fixed and α_i and/or σ_i^2 varied.
361 Although CID+ models did not garner much support when these models were fit, OU1 and BM1
362 models served as reasonable null hypotheses in these cases. In general, we found that when CID
363 models were the generating model, evidence of CID was strongest and when CD models were
364 the generating model, evidence of character dependence was strongest. This suggests that the
365 effect of rate heterogeneity causing false correlations is not as pronounced as other comparative
366 methods (Maddison and FitzJohn 2015; Rabosky and Goldberg 2015).

367

368 *Seed dispersal and climatic evolution*

369 We found evidence of a character-dependent model over either a simple or hidden state
370 character-independent model, suggesting a link between the climatic niche of Ericaceae lineages
371 and their fruit type (Table S2). The best supported models were OUMVA and OUVA with AIC
372 weights of 0.41 and 0.32 respectively. This suggests that there were character dependent
373 differences in phenotypic optima, rates of evolution, and overall phylogenetic signal. To evaluate
374 support for our hypotheses we examined the model averaged parameter estimates (Table 4). The

375 estimated optimum $0.81 \ln(AI) (\pm 0.28)$ for fleshy fruits suggests a more arid environment for
376 their optimal habitat, and the $0.97 \ln(AI) (\pm 0.011)$ of dry fruits corresponds to a more humid
377 environment (Middleton and Thomas 1997), where AI is measured as mean annual precipitation
378 (P) divided by average annual potential evapotranspiration (PET). However, both optima
379 correspond to non-dryland humid environments. Both σ^2 and α interact to create tip variance, so
380 in addition to σ^2 , we measured the stationary variance $V = \frac{\sigma^2}{2\alpha}$. As predicted, we found that
381 Ericaceae lineages with dry fruits were more variable in their climatic niche evolution ($\sigma_{dry}^2 =$
382 $0.011 \ln(AI)^2 MY^{-1}$, $V_{dry} = 0.37 \ln(AI)^2$) compared to fleshy fruits ($\sigma_{fleshy}^2 =$
383 $0.007 \ln(AI)^2 MY^{-1}$, $V_{fleshy} = 0.15 \ln(AI)^2$). Additionally, the strength of pull of fleshy fruited
384 lineages was greater than dry fruited lineages ($\alpha_{fleshy} = 0.022 MY^{-1} > \alpha_{dry} = 0.014 MY^{-1}$).
385 This corresponds to phylogenetic half-lives of $t_{1/2,dry} = 46.4 MY$ and $t_{1/2,fleshy} = 30.3 MY$
386 which are 38% and 25% of the total tree height respectively. Transitions to fleshy fruit occurred
387 at 0.0015 transitions per million years which is more than 4.3 times faster than transitions to dry
388 fruits (0.0004 transitions per million years). The waiting time $\left(\frac{1}{q}\right)$ of fleshy fruits (2,500 MY)
389 was substantially longer than that of dry fruits (667 MY). Given that the total branch length in
390 the tree is 10,120 MY, we expect that lineages were typically under the fleshy fruit regime and
391 evolving towards a preference for more humid environments. Perhaps for this reason we found
392 that, on average, lineages were in more arid environments than predicted by the model (average
393 difference of 0.19 AI), with some species expected to be in much more humid environments
394 (difference between current AI and optimal AI ranged from -4.4 to 0.85).

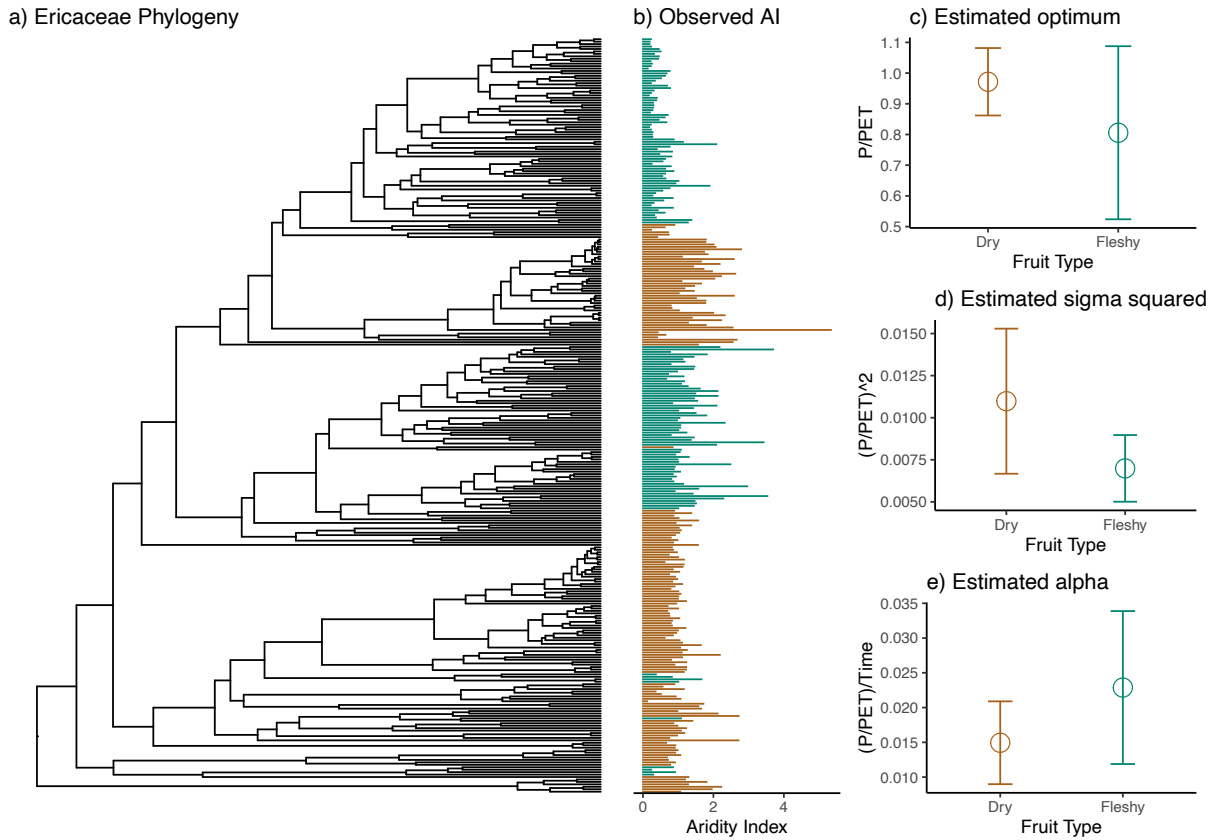


Figure 4. a) Ericaceae phylogeny for which we had data (n=309). b) Ln aridity index dataset where each bar is colored by dry (brown) and fleshy (green) fruit type. c) Model averaged parameter estimates with standard error calculated from 100 parametric bootstraps.

396

397 **Table 4.** Model averaged parameter estimates and standard errors for Ericaceae aridity index and
 398 fruit type data. Models with higher AIC weights contribute more overall to the parameter values.

399 The units for α , σ^2 , and θ are $\frac{P}{PET} \div time$, $\left(\frac{P}{PET}\right)^2$, and $\frac{P}{PET}$ respectively. P is the average annual
 400 precipitation and PET is average annual potential evapotranspiration. Rates of q are measured in
 401 transitions per million years.

Continuous parameter estimates				Discrete parameter estimates	
	α	σ^2	θ		
Dry	0.015 (± 0.0059)	0.011 (± 0.0043)	0.97 (± 0.011)	$q_{dry\ to\ fleshy}$	0.0015 (± 0.00058)
Fleshy	0.023 (± 0.011)	0.007 (± 0.002)	0.81 (± 0.28)	$q_{fleshy\ to\ dry}$	0.0036 (± 0.000086)

402

403

404

Discussion

405 Phylogenetic comparative methods have been widely applied to study discrete and
406 continuous characters separately. Due primarily to computational limitations there are few
407 options which jointly evaluate both classes of character. The *hOUwie* framework proposed here
408 overcomes these limitations, and we demonstrate how it is used to test hypotheses of correlated
409 evolution between discrete and continuous characters while accounting for hidden character
410 states and unobserved variation. Our model jointly models discrete and continuous characters by
411 linking both via a common regime painting. However, unlike other similar methods, our
412 likelihood formula explicitly calculates the probability of the underlying regimes. This has the
413 advantage of describing the discrete character evolution probabilistically and allows information
414 from the discrete and continuous characters to jointly contribute to the overall likelihood.

415

416

Relationship to existing methods

417 Considerable progress has been made towards more realistic models of continuous
418 character evolution within the last two decades. Continuous character models which initially
419 relied on either single rate Brownian motion or simple Ornstein-Uhlenbeck models (Felsenstein
420 1985; Hansen 1997) have seen several extensions to allow for heterogeneity in the evolutionary
421 process as well as the deterministic influence of underlying independent variables. Generally,
422 these models can be classified as either being “hypothesis driven” or “data driven” (Martin et al.
423 2022). Hypothesis driven models are those which require *a priori* hypotheses regarding where
424 evolutionary rates may differ throughout the phylogeny. These include models which have
425 extended simple single-rate BM to incorporate rate variation based on discrete regime mappings
426 (e.g., O’Meara et al. 2006; Thomas et al. 2006; Revell and Collar 2009; Caetano and Harmon

427 2017) or more generalized Ornstein-Uhlenbeck models where parameters are allowed to vary
428 based on an underlying regime mapping (e.g., Butler and King 2004; Bartoszek et al. 2012;
429 Beaulieu et al. 2012). In contrast, several methods have focused on the development of data
430 driven, shift-detection methods (which may indeed be used in testing hypotheses, but these
431 hypotheses are not directly used in creating the regime map). These methods utilize an Ornstein-
432 Uhlenbeck process to automatically detect where in the phylogeny evolutionary rates and
433 phenotypic optima shift (Ingram and Mahler 2013b; Uyeda and Harmon 2014; Khabbazian et al.
434 2016; Bastide et al. 2017). Furthermore, some recently developed methods have allowed for rate
435 variation without the assumption of constant regimes at all. Instead, these models assume the
436 rates themselves evolve and change throughout the phylogeny under various Brownian motion-
437 like processes (Lemey et al. 2010; Eastman et al. 2013; Revell 2021; Martin et al. 2022) or single
438 optima Ornstein-Uhlenbeck processes (Hansen et al. 2008; Mitov et al. 2019). The method
439 presented here is most like the latter group. *hOUwie* attempts to explicitly model the evolution of
440 rate shifts according to regimes which jointly influence discrete and continuous character
441 evolution. The regimes themselves are never fixed a priori and each is evaluated as a partial
442 contribution to the overall probability of the data. The advantage of this approach is that it
443 acknowledges the uncertainty in the underlying regime paintings and allows them to change
444 through time.

445 Additionally, unlike *hOUwie*, the “hypothesis driven” or “data driven” models do not
446 explicitly account for the joint modeling of the discrete and continuous characters. Most progress
447 in this area has, until recently, been made via phylogenetic logistic regressions (Ives and Garland
448 2010) or threshold models in which the discrete character is modeled by a continuously varying
449 unobserved liability (Felsenstein 2012; Revell 2014; Cybis et al. 2015). However, these models

450 rely on more simplistic evolutionary models without character independent rate heterogeneity
451 (such as single rate Brownian motion). This lack of character independent rate heterogeneity has
452 recently been recognized as a potential source of inflated correlation between discrete and
453 continuous characters. Such was the reasoning for the MuSSCRat model (May and Moore 2020).
454 Like *hOUwie*, MuSSCRat allows for character-independent rate heterogeneity following a
455 multiple rate Brownian motion model to be directly contrasted against character correlation to
456 correct for potential biases towards correlation. However, the way the underlying discrete
457 character is calculated in *hOUwie*, as well as how rate heterogeneity is modeled, differs
458 substantially from May and Moore (2020). Finally, Tribble et al. (2021) has recently developed a
459 method which is similar to the one presented here. One of the primary differences between
460 *hOUwie* and the Bayesian pipeline discussed in Tribble et al. (2021) is how discrete character
461 evolution is treated. Specifically, Tribble et al. (2021) assumed that character-independent
462 mappings are generated under the same parameters which best fit their focal discrete character.
463 In contrast, *hOUwie* allows the free estimation of character-independent discrete rates which best
464 fit both discrete and continuous data. This difference may lead to biases against null models in
465 the Tribble et al. (2021) approach since the character-independent regimes are forced to follow a
466 character-dependent discrete model.

467

468 *Character-independent models and null hypotheses*

469 There is a growing appreciation that comparing constant-rate null models to variable-rate
470 alternative models will consistently favor rate heterogeneity, regardless of whether there is a
471 genuine association with a focal variable (Maddison and FitzJohn 2015; Rabosky and Goldberg
472 2015; Beaulieu and O'Meara 2016; Uyeda et al. 2018; O'Meara and Beaulieu 2021; Boyko and

473 Beaulieu 2022). This problem, termed the “straw-man effect” by May and Moore (2020), has
474 been demonstrated to lead to nearly 100% error rates for evidence of discrete character
475 correlation (Maddison and FitzJohn 2015; Boyko and Beaulieu 2022), and has severely biased
476 evidence towards state-dependent speciation and extinction (Rabosky and Goldberg 2015;
477 Beaulieu and O’Meara 2016). Given these often-overwhelming error rates in other comparative
478 methods, we expected to find a similarly consistent bias towards correlation between discrete and
479 continuous characters. However, we found that support for single rate character-independent null
480 models was greater than character-dependent models even when simulated under character-
481 independent models with rate heterogeneity. Although the inclusion of explicit multi-rate
482 character independent models (CID+) models did help reduce evidence of false correlation in
483 some cases, by and large, simplistic null models performed admirably. This is not to say that the
484 error rates for discrete and continuous character correlation should be dismissed outright. If our
485 simulations correctly assess that nearly one-third of results find false evidence of a correlation
486 between continuous character rates of evolution and discrete characters, then better null models
487 are certainly needed. But, in comparison to the profound effect that model misspecification has
488 had in other comparative analyses (Beaulieu and O’Meara 2016; Boyko and Beaulieu 2022), the
489 joint models tested here have substantially lower error rates.

490 We suspect that part of the reason that the correlation between discrete and continuous
491 characters is less susceptible to “straw-man” effects than other PCMs is related to the
492 inefficiency of sampling potential maps from the univariate stochastic mapping model. A
493 common approach to fitting OU models involves simulating many stochastic maps to represent
494 underlying regimes from parameters estimated only from the discrete character (Revell 2013).
495 The resulting distribution of underlying regimes will therefore reflect a distribution appropriate

496 for the discrete character, but not necessarily suitable for the continuous character. This is
497 especially true if the continuous character is unlinked to the focal discrete character. Indeed, we
498 found that if the discrete and continuous characters are unlinked, most stochastic maps, even
499 though good descriptions of the discrete characters, were completely inadequate representations
500 of continuous regimes. Thus, any joint model with these maps contributed little to the overall
501 likelihood. Under our simulation protocol, for a typical run, 90% of the total likelihood for the
502 best set of parameters came from just 2% of the attempted maps.

503 In some ways the substantial contributions of only a few underlying regimes to the
504 overall likelihood is good. First, it makes spurious links between a randomly distributed discrete
505 character and a continuous character more unlikely since associations between regimes and
506 continuous variables tend to be specific. This ultimately reduces the potential “straw-man”
507 effect. Second, the continuous characters can inform the placement of shared regimes and
508 therefore shift detection methods, where the continuous data are all that provides information
509 about regimes shifts (Ingram and Mahler 2013; Uyeda and Harmon 2014; Khabbazian et al.
510 2016; Bastide et al. 2017), may be appropriate across a broad range of scenarios. However, this
511 property also makes sampling a good set of regimes to get an accurate estimate of the likelihood
512 difficult and is why the development of our adaptive sampling heuristics was necessary.
513 Adaptive sampling, in combination with our approximation of the joint conditional distributions,
514 helped make parameter estimation more accurate. Increasing the amount of sampled regime
515 mappings is useful in improving precision (Fig. S1), at the cost of longer run time.

516

517

518

519
520
521
522
523
524
525
526
527
528
529
530
531
532
533
534
535
536
537
538
539
540
541

Interplay of continuous, discrete, and hidden traits

In many studies that deal with the correlation of discrete and continuous traits, it is often assumed that the discrete trait functions as the independent trait and the continuous trait as the dependent trait. This assumption is baked into methods that map the discrete trait first and then analyze the continuous trait given these mappings, but it would be easy to fall into this form of thinking even with *hOUwie*, which does not have this assumption. Instead, *hOUwie* can help understand whether and how traits are correlated. For example, one could see if mammal body size correlates with trophic level: are hypercarnivores larger on average than herbivores? It could be that an herbivorous (discrete character) beaver evolves a taste for meat and then grows bigger (continuous character) so it can take down bigger prey; it could be that once things get to be the size of a bison (continuous character) they start adding more and more rodents to their diet, eventually becoming carnivores (discrete character). Causality can go both directions, and of course both traits may be evolving based on some other third trait and not functionally related to each other.

hOUwie is part of a series of hidden state models developed by our research groups (i.e., Beaulieu et al. 2013; Beaulieu and O’Meara 2016; Caetano et al. 2018; Boyko and Beaulieu 2021, 2022; Vasconcelos et al. 2022). One misconception we have noted in use of these methods is the thought that there is a single, discrete, hidden character in the biology. These models do model a single hidden character (with potentially many states), but this could be reflecting multiple characters evolving together or other factors that change in a heritable manner through time. It is a way to allow heterogeneity, especially by factors that vary by clades. With *hOUwie*, this heterogeneity can affect the discrete trait, the continuous trait, both, or neither.

542

Seed dispersal and climatic niche evolution in Ericaceae

543

Here we reevaluated three hypotheses related to climatic niche evolution and seed

544

dispersal and found that: (1) the climatic optima of dry fruits was more humid than fleshy fruits

545

($\theta_{fleshy} < \theta_{dry}$), (2) lineages with dry fruits had faster rates of climatic niche evolution ($\sigma_{dry}^2 >$

546

σ_{fleshy}^2), and (3) climatic niches of fleshy fruits are more conserved through time ($\alpha_{dry} <$

547

α_{fleshy}). In contrast to previous findings, the higher rate and stationary variance of climatic niche

548

evolution for dry seeds matched our original hypothesis (Vasconcelos et al. 2021). This is to be

549

expected because abiotically dispersed seeds are likely to be more erratic in their dispersal

550

patterns (Schupp 1993; Westoby et al. 1996). Additionally, that our results differ from previous

551

findings (Vasconcelos et al. 2021) suggests that jointly modeling climatic niche evolution

552

alongside fruit type changed our parameter estimation in a meaningful way.

553

Our final hypothesis, which stated that fleshy, biotically dispersed, seeds are more likely

554

to be associated with humid environments, was not supported. However, it has been suggested

555

that a trade-off between seed persistence, seed size, and dispersal strategies can be also common

556

in arid environments (Venable and Brown 1988; Nunes et al. 2017). Specifically, large seed size

557

may occasionally help withstand unfavorable conditions associated with increased aridity (Nunes

558

et al. 2017). With an increased seed size, biotic seed dispersal and fleshy fruits, may become

559

necessary for seed dispersal. This may be the case for Styphelieae, which is distributed in the

560

arid Australian heathland and, of all predominately fleshy-fruited groups, lies the furthest from

561

the inferred aridity optima. Additionally, it has been found that the proportion of abiotically

562

dispersed seeds increases as elevation increases, due to the decreasing availability of frugivores

563

(Chapman et al. 2016). Given that several radiations of Ericaceae lineages are associated with

564

montane habitats (Schwery et al. 2015), it may be that the distribution of dry and fleshy fruits are

565 a consequence of elevation rather than being directly linked to climatic niche evolution. Finally,
566 it has been noted Ericaceae lineages are often found in well-leached soils and epiphytic habitats
567 (Schwery et al. 2015). If associations with soil type are more important than links to climatic
568 optima, we may expect that fruit-dependent climatic optima are consequence of unmodeled
569 factors. Although our modeling explicitly considers hidden variables that may lead to rate
570 heterogeneity, if the proposed hidden variable (soil condition) is closely linked to our modeled
571 variable (aridity), then we may not be able to detect the presence of hidden variation. This may
572 be the case between soil condition and aridity (Moreno-Jiménez et al. 2019).

573

574 *Caveats and possible extensions*

575 There are three important caveats to our proposed modeling framework. First, our
576 discrete mapping probability, $P(D, z|\vartheta, \psi)$, is only an approximation. What we calculate is the
577 probability of starting in a particular state i and ending a particular state j , summed over all
578 possible paths. However, the continuous model probability is based off a particular pathway
579 history that is defined throughout the entire branch (Hansen 1997). Ultimately, this means that
580 the underlying regimes are not treated identically for the continuous and discrete characters. The
581 second caveat is that we do not force $hOUwie$ to sum over all possible mappings z . This is
582 because the number of mappings will grow exponentially as the number of nodes and internodes
583 increases and the computation will quickly become infeasible (see Jones et al. 2020). Although
584 this may not be entirely necessary since we have shown that only a small percentage of possible
585 mappings contribute to the overall joint probability. Nonetheless, an ideal solution could be the
586 use Markov-Modulated Ornstein-Uhlenbeck models (Huang et al. 2016) since this would remove
587 the need for a regime mapping approach, but these have yet to be applied in phylogenetic

588 comparative biology. *hOUwie* currently only deals with one discrete and one continuous trait at a
589 time – a set of discrete traits can be handled by converting them to a single multistate character,
590 but incorporating multiple continuous traits requires adding correlations between them. Finally,
591 it is possible to extend *hOUwie* to include state-dependent speciation and extinction dynamics
592 which have been shown to influence the distribution of discrete characters (Maddison 2006) and
593 would therefore influence continuous characters if the two were linked. However, this extension
594 would require a different calculation of the underlying regime mapping probability. Approaches
595 for stochastically mapping SSE models already exist (Freyman and Höhna 2019), so the largest
596 remaining challenge of this extension would be generating high joint probability mappings.

597

598

Concluding remarks

599

600

601

602

603

604

605

606

607

The use of pre-defined discrete character mappings can be useful for testing hypotheses which rely on distinct, well-defined differences in the evolutionary histories of lineages. However, this approach assumes that the underlying mapping is known with complete accuracy and ignores the probabilistic nature of discrete regimes. *hOUwie*'s methodology integrates over the uncertainty of high probability character mappings and relies on the interpretation of parameter estimates from contrasting model structures to find evidence for hypotheses. Rather than assuming an *a priori* mapping, *hOUwie* can utilize the mutual information about the discrete and continuous characters to learn something about the underlying regimes evolution.

609 **Table 1.** A comparison of the effectiveness of the adaptive sampling procedure and standard
610 discrete only sampling of maps. Regardless of the sampling procedure, all probabilities are
611 calculated in the same way and so any differences in probabilities reflects each procedure's
612 ability to generate appropriate mappings. 50 regime mappings are used to calculate the likelihood
613 of the parameters. A higher \log_e likelihood is better (that is, -16.43 is better than -16.48; 10.54 is
614 better than 9.19) For each model type, data are simulated following our methods with $q_{ij} =$
615 $0.1, \alpha_1 = 3, \alpha_2 = 1.5, \sigma_1^2 = 0.35, \sigma_2^2 = 1, \theta_1 = 2,$ and $\theta_2 = 0.75$. The generating parameters are
616 used to evaluate probability of each dataset and thus the probabilities represented here are not
617 necessarily the same as those derived from the MLE. Generally, adaptive sampling improves the
618 joint estimate by improving the probability of the continuous character and is most effective for
619 variable θ models. As expected, discrete only sampling produces regime paintings which better
620 reflect the discrete character than adaptive sampling, but the difference is minor.
621

Model class	Model type	Sampling procedure	Discrete marginal \log_e likelihood	Continuous marginal \log_e likelihood	Joint \log_e likelihood
CID+	BMV	adaptive sampling	-16.48	10.54	-10.59
		discrete only	-16.43	9.19	-10.59
	OUA	adaptive sampling	-15.46	44.34	25.14
		discrete only	-15.53	43.11	24.96
	OUV	adaptive sampling	-30.89	47.86	12.17
		discrete only	-30.14	46.00	12.11
	OUVA	adaptive sampling	-11.88	36.91	21.14
		discrete only	-11.17	36.27	21.08
	OUM	adaptive sampling	-11.94	57.57	39.08
		discrete only	-11.19	53.56	32.21
	OUMA	adaptive sampling	-9.94	35.01	17.39
		discrete only	-9.38	2.19	-20.48
	OUMV	adaptive sampling	-19.96	20.77	-15.64
		discrete only	-14.76	-2.92	-25.83
	OUMVA	adaptive sampling	-13.91	25.47	7.48
		discrete only	-13.23	26.36	4.48
	OUBM1	adaptive sampling	-14.26	42.20	24.39
		discrete only	-14.88	40.89	24.22
	OUBMV	adaptive sampling	-19.17	49.10	18.84
		discrete only	-19.01	33.45	7.71

622

623

624

625

626 **Table 2.** The average accuracy of *hOUwie* parameter estimates across several model classes and
627 types as measured by root-mean-square error (RMSE). RMSE is calculated for each model type
628 by taking the square root of the mean squared error (MSE), where MSE is the average squared
629 difference between the MLE and the simulating parameters. Data is generated with $q_{ij} =$
630 $0.1, \alpha_1 = 3, \alpha_2 = 1.5, \sigma_1^2 = 0.35, \sigma_2^2 = 1, \theta_1 = 2,$ and $\theta_2 = 0.75,$ and for phylogenies with 25,
631 100, and 250 taxa. Finally, model fits use either 25, 100, or 250 stochastic maps per likelihood
632 iteration. The table shown here calculates RMSE integrating over all phylogenetic tree sizes and
633 number of stochastic maps (n=8217). Dashes indicate a parameter that is not estimated for a
634 given model type. Generally, character independent (CID+) models had higher errors than
635 character dependent (CD) models. The greatest errors occurred when estimating alpha in variable
636 alpha models for both CD and CID+ model classes. Estimates of the optimum and transition
637 rates generally had the lowest errors.

Model class	Model type	RMSE q	RMSE α_1	RMSE α_2	RMSE σ_1^2	RMSE σ_2^2	RMSE θ_1	RMSE θ_2
CD	BMV	0.12	-	-	0.10	0.28	0.22	-
	OUV	0.11	1.27	-	0.15	0.33	0.05	-
	OUA	0.12	1.55	1.63	0.11	-	0.06	-
	OUM	0.13	1.49	-	0.10	-	0.07	0.13
	OUVA	0.09	1.44	1.11	0.14	0.98	0.06	-
	OUMV	0.16	1.82	-	0.16	0.32	0.07	0.17
	OUMA	0.15	2.11	2.48	0.28	-	0.12	0.50
	OUMVA	0.18	1.62	1.12	0.12	1.07	0.76	1.06
	OUBM1	0.1	2.64	-	0.08	-	0.08	-
	OUBMV	0.09	2.29	-	0.13	2.37	0.08	-
CID+	BMV	0.05	-	-	0.27	10.11	0.24	-
	OUV	0.04	1.13	-	0.32	1.83	0.05	-
	OUA	0.05	2.93	1.34	0.33	-	0.07	-
	OUM	0.09	2.53	-	0.15	-	0.44	0.20
	OUVA	0.05	1.26	1.11	0.27	13.44	0.07	-
	OUMV	0.1	2.50	-	0.16	2.12	1.30	0.68
	OUMA	0.05	8.28	1.27	0.23	-	5.88	0.8
	OUMVA	0.07	5.54	1.24	0.20	9.37	8.76	1.35
	OUBM1	0.05	3.33	-	0.32	-	0.14	-
	OUBMV	0.05	3.50	-	0.27	8.79	0.14	-

638

639

640

641

642

643 **Table 3.** Average AIC weight as the number of taxa increases for each model class. Gray cells
 644 indicate the AIC weight of the generating model class. In general, as the number of taxa
 645 increases the average support for the generating model class increases.

Generating model class	nTaxa	AICwt BM1	AICwt OU1	AICwt CD	AICwt CID+
CD	25	0.12	0.22	0.51	0.15
	100	0.06	0.22	0.70	0.02
	250	0.02	0.14	0.82	0.02
CID+	25	0.28	0.35	0.24	0.14
	100	0.21	0.4	0.23	0.15
	250	0.11	0.34	0.32	0.22

646

647

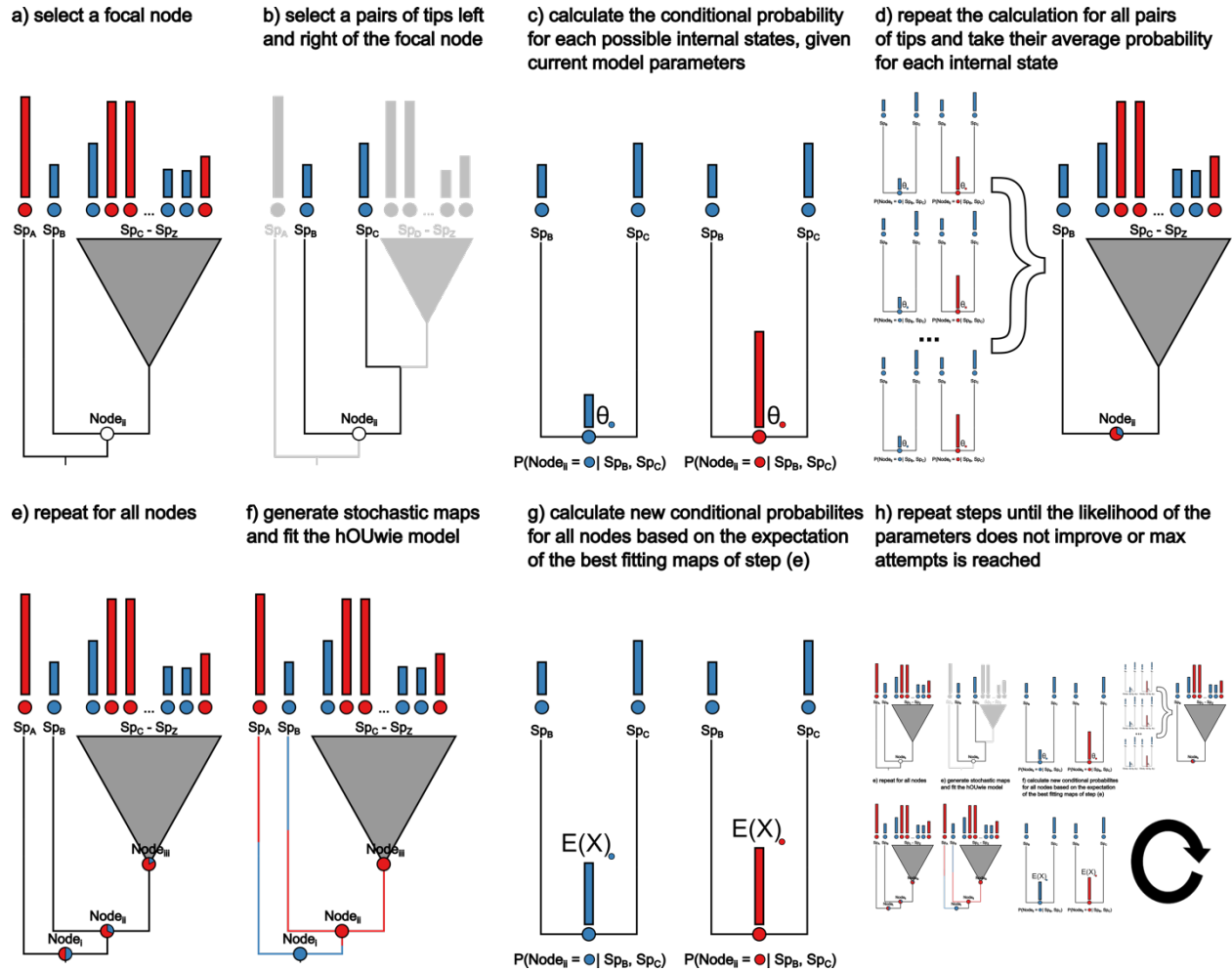
648 **Table 4.** Model averaged parameter estimates and standard errors for Ericaceae aridity index and
 649 fruit type data. Models with higher AIC weights contribute more overall to the parameter values.

650 The units for α , σ^2 , and θ are $\frac{P}{PET} \div time$, $\left(\frac{P}{PET}\right)^2$, and $\frac{P}{PET}$ respectively. P is the average annual
 651 precipitation and PET is average annual potential evapotranspiration. Rates of q are measured in
 652 transitions per million years.

	Continuous parameter estimates			Discrete parameter estimates	
	α	σ^2	θ		
Dry	0.015 (± 0.0059)	0.011 (± 0.0043)	0.97 (± 0.011)	$q_{dry\ to\ fleshy}$	0.0015 (± 0.00058)
Fleshy	0.023 (± 0.011)	0.007 (± 0.002)	0.81 (± 0.28)	$q_{fleshy\ to\ dry}$	00036 (± 0.000086)

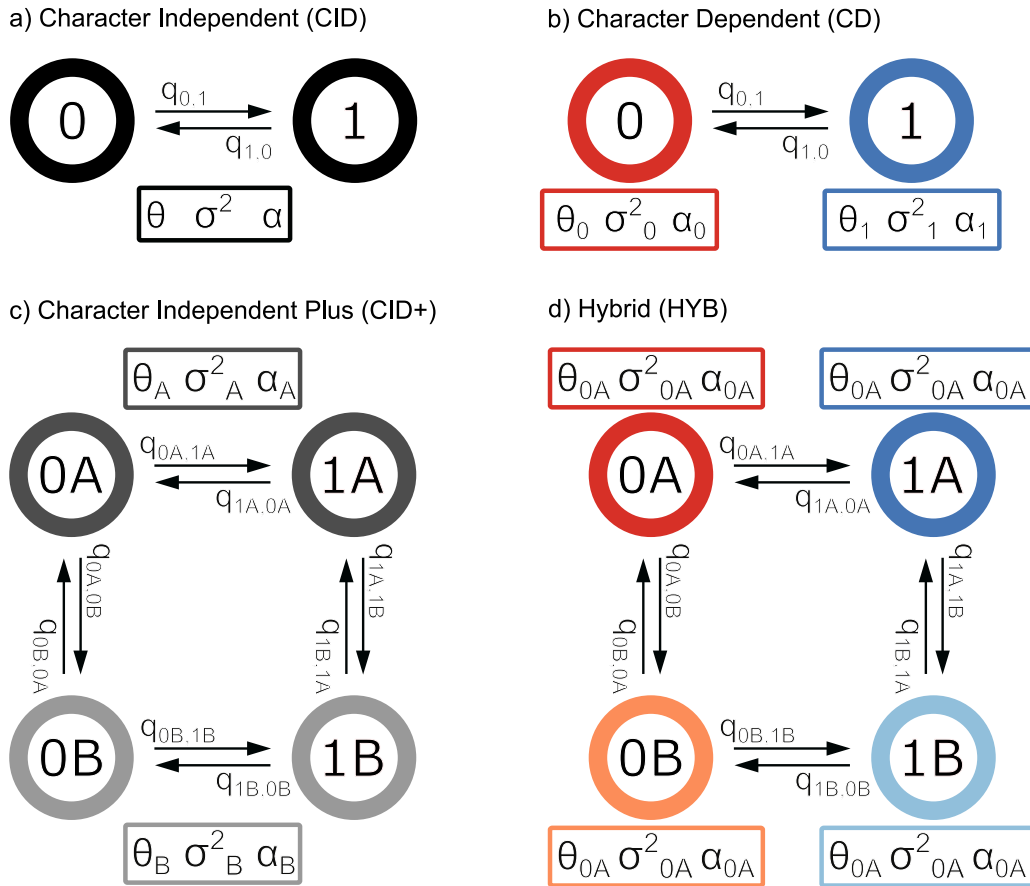
653

Figures



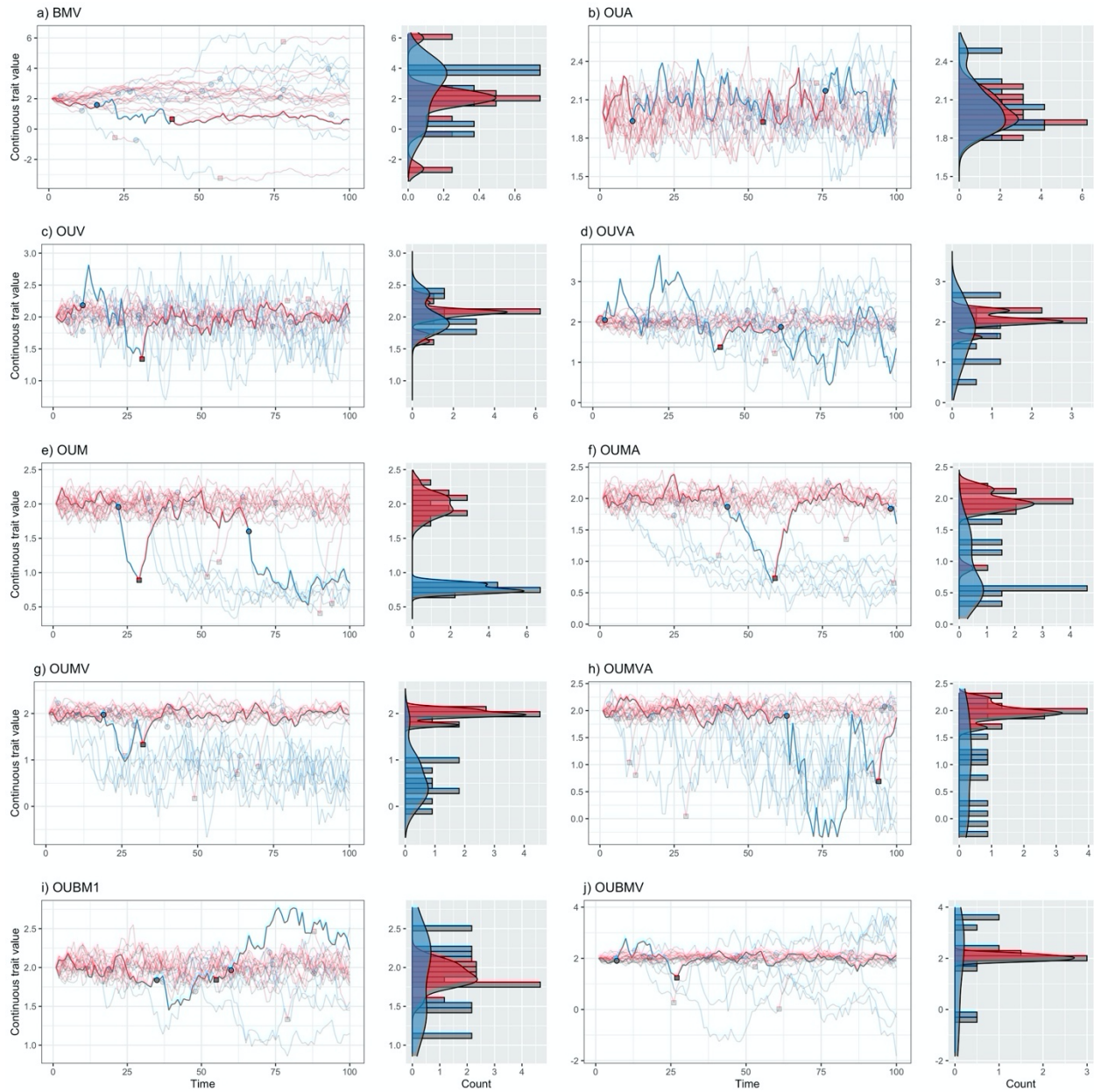
655

656 **Figure 1.** A visual representation of the algorithm underlying the calculation of conditional node
 657 probabilities and the adaptive sampling procedure. The goal of the procedure is to produce
 658 underlying regime paintings well suited to both the discrete and continuous character. a) select
 659 the focal node for which we will be calculating the joint conditional probabilities of the discrete
 660 and continuous characters. b) on each side of the node we select a pair of tips. c) the conditional
 661 probability of the observed discrete and continuous character is calculated for each discrete
 662 regime state with an ancestral continuous value equal to θ of that regime state. d) the conditional
 663 probability of the focal node is calculated as the average probability of each regime state for all
 664 pairs of observed tips. e) the conditional probabilities are calculated for all internal nodes. This
 665 can be turned off within *hOUwie* by setting the *sample_nodes* argument to false. f) A stochastic
 666 map is generating using forward simulation rejection sampling. g) adaptive sampling uses the
 667 highest joint probability of previously generated underlying regimes to generate a set of ancestral
 668 continuous character values. This differs from previous ancestral values because instead of
 669 assuming the value θ for each regime state, it calculates the expected value given the root state
 670 and regime mapping for that particular node. h) we repeat steps d) through g) until the joint
 671 likelihood of the set of underlying regimes does not improve.
 672



673

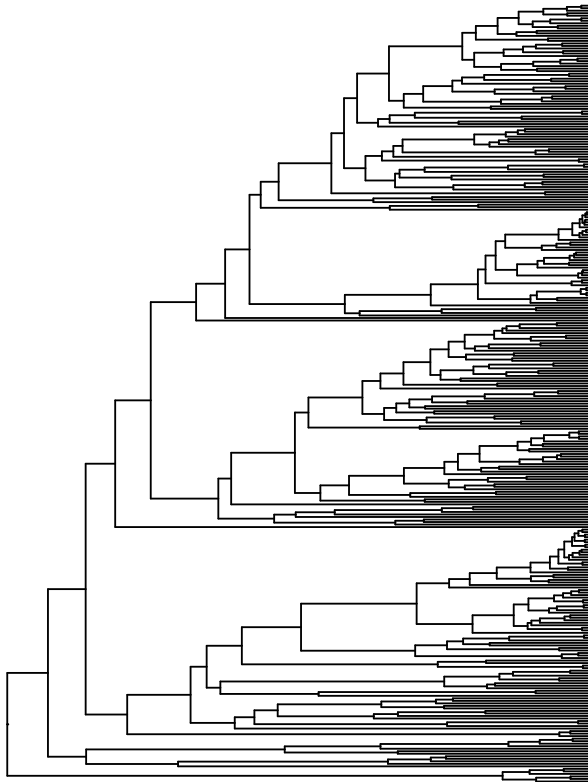
674 **Figure 2.** A state-transition diagram describing the model classes allowable in hOUwie. Each
 675 panel is comprised of observed discrete states 0 and 1 with possible hidden states A and B.
 676 Transitions between states are described with the q parameter. Continuous model parameters
 677 appear in a box below the states they describe, and their association is displayed with a subscript
 678 specific to that state. a) A simple character independent model in which the two observed states
 679 do not influence the continuous character which will have the same θ , σ^2 , α throughout the
 680 phylogeny. b) A character dependent model in which the continuous character depends on the
 681 discrete character by virtue of θ , σ^2 , α being associated with a particular observed discrete state.
 682 c) A character independent model with rate heterogeneity. The two observed states (0 and 1) are
 683 not directly linked to the continuous character. However, the continuous character is still allowed
 684 to have multiple θ , σ^2 , α describing its evolution, but these parameters are associated with
 685 hidden states A and B. d) A hybrid model in which each combined observed and hidden state is
 686 allowed to have its own θ , σ^2 , α . Under this model, the continuous character is linked to both
 687 character dependent differences (parameters associated with 0 and 1) and character independent
 688 differences (A and B). Though this diagram shows a binary observed and hidden character, either
 689 can have more states (up to 26 states for each in theory, though few datasets will have enough
 690 power to estimate the necessary number of parameters).
 691



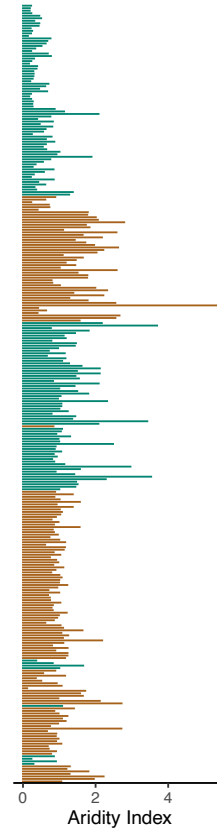
692

693 **Figure 3.** A visual representation of binary discrete character *hOUwie* model types. Discrete
 694 time forward simulations are conducted starting in the red state and the distribution of the
 695 continuous character is plotted on the right as a histogram and density plot. Each line represents
 696 a continuous character value at some time. Transitions occur at colored points and each line is
 697 colored by the current discrete state. 100 time-steps are simulated with the same parameters as
 698 our simulation study ($q_{ij} = 0.1$, $\alpha_1 = 3$, $\alpha_2 = 1.5$, $\sigma_1^2 = 0.35$, $\sigma_2^2 = 1$, $\theta_1 = 2$, and $\theta_2 = 0.75$).
 699 The highlighted line was randomly chosen from the set in which at least one discrete state
 700 transition occurred.

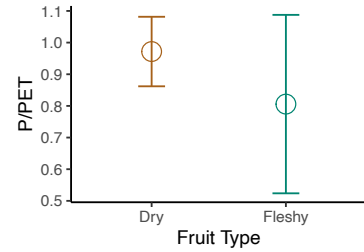
701 a) Ericaceae Phylogeny



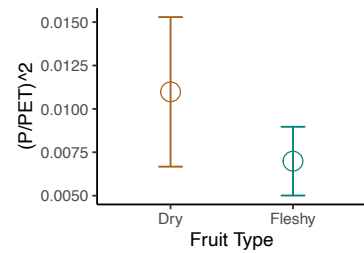
b) Observed AI



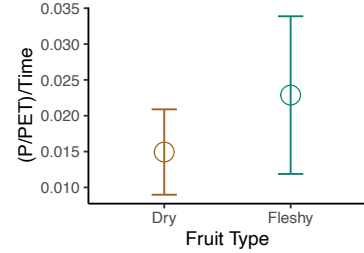
c) Estimated optimum



d) Estimated sigma squared



e) Estimated alpha



702

703 **Figure 4.** a) Ericaceae phylogeny for which we had data (n=309). b) Ln aridity index dataset
704 where each bar is colored by dry (brown) and fleshy (green) fruit type. c) Model averaged
705 parameter estimates with standard error calculated from 100 parametric bootstraps.

- 707 Bartoszek K., Pienaar J., Mostad P., Andersson S., Hansen T.F. 2012. A phylogenetic
708 comparative method for studying multivariate adaptation. *Journal of Theoretical Biology.*
709 314:204–215.
- 710 Bastide P., Mariadassou M., Robin S. 2017. Detection of adaptive shifts on phylogenies by using
711 shifted stochastic processes on a tree. *Journal of the Royal Statistical Society: Series B*
712 (Statistical Methodology). 79:1067–1093.
- 713 Beaulieu J.M., Jhweng D.-C., Boettiger C., O’Meara B.C. 2012. Modeling Stabilizing
714 Selection: Expanding the Ornstein–Uhlenbeck Model of Adaptive Evolution. *Evolution.*
715 66:2369–2383.
- 716 Beaulieu J.M., O’Meara B.C. 2016. Detecting Hidden Diversification Shifts in Models of Trait-
717 Dependent Speciation and Extinction. *Syst Biol.* 65:583–601.
- 718 Beaulieu J.M., O’Meara B.C., Donoghue M.J. 2013. Identifying Hidden Rate Changes in the
719 Evolution of a Binary Morphological Character: The Evolution of Plant Habit in
720 Campanulid Angiosperms. *Syst Biol.* 62:725–737.
- 721 Boyko, J., & Beaulieu, J. M. (2022, April 1). Reducing the biases in false correlations between
722 discrete characters. <https://doi.org/10.32942/osf.io/e2kj8>
- 723 Boyko J.D., Beaulieu J.M. 2021. Generalized hidden Markov models for phylogenetic
724 comparative datasets. *Methods Ecol Evol.* 12:468–478.
- 725 Burnham K.P., Anderson D.R. 2002. Model selection and multimodel inference: a practical
726 information-theoretic approach. New York: Springer.
- 727 Butler M.A., King A.A. 2004. Phylogenetic Comparative Analysis: A Modeling Approach for
728 Adaptive Evolution. *The American Naturalist.* 164:683–695.
- 729 Caetano D.S., Harmon L.J. 2017. ratematrix: An R package for studying evolutionary integration
730 among several traits on phylogenetic trees. *Methods in Ecology and Evolution.* 8:1920–
731 1927.
- 732 Caetano D.S., O’Meara B.C., Beaulieu J.M. 2018. Hidden state models improve state-dependent
733 diversification approaches, including biogeographical models: HMM and the adequacy of
734 SSE models. *Evolution.* 72:2308–2324.
- 735 Chapman H., Cordeiro N.J., Dutton P., Wenny D., Kitamura S., Kaplin B., Melo F.P.L., Lawes
736 M.J. 2016. Seed-dispersal ecology of tropical montane forests. *Journal of Tropical*
737 *Ecology.* 32:437–454.
- 738 Cressler C.E., Butler M.A., King A.A. 2015. Detecting Adaptive Evolution in Phylogenetic
739 Comparative Analysis Using the Ornstein–Uhlenbeck Model. *Systematic Biology.*
740 64:953–968.

- 741 Cybis G.B., Sinsheimer J.S., Bedford T., Mather A.E., Lemey P., Suchard M.A. 2015.
742 ASSESSING PHENOTYPIC CORRELATION THROUGH THE MULTIVARIATE
743 PHYLOGENETIC LATENT LIABILITY MODEL. *Ann Appl Stat.* 9:969–991.
- 744 Eastman J.M., Wegmann D., Leuenberger C., Harmon L.J. 2013. Simpsonian “Evolution by
745 Jumps” in an Adaptive Radiation of Anolis Lizards. arXiv:1305.4216 [q-bio].
- 746 Felsenstein J. 1985. Phylogenies and the Comparative Method. *Am. Nat.* 125:1–15.
- 747 Felsenstein J. 2004. *Inferring phylogenies*. Sinauer associates Sunderland, MA.
- 748 Felsenstein J. 2012. A Comparative Method for Both Discrete and Continuous Characters Using
749 the Threshold Model. *The American Naturalist.* 179:145–156.
- 750 Foster S., Janson C.H. 1985. The relationship between seed size and establishment conditions in
751 tropical woody plants. *Ecology.* 66:773–780.
- 752 Freyman W.A., Höhna S. 2019. Stochastic Character Mapping of State-Dependent
753 Diversification Reveals the Tempo of Evolutionary Decline in Self-Compatible
754 Onagraceae Lineages. *Systematic Biology.* 68:505–519.
- 755 Hansen T.F. 1997. Stabilizing Selection and the Comparative Analysis of Adaptation. *Evolution.*
756 51:1341–1351.
- 757 Hansen T.F. 2014. Use and Misuse of Comparative Methods in the Study of Adaptation. In:
758 Garamszegi L.Z., editor. *Modern Phylogenetic Comparative Methods and Their*
759 *Application in Evolutionary Biology*. Berlin, Heidelberg: Springer Berlin Heidelberg. p.
760 351–379.
- 761 Hansen T.F., Pienaar J., Orzack S.H. 2008. A Comparative Method for Studying Adaptation to a
762 Randomly Evolving Environment. *Evolution.* 62:1965–1977.
- 763 Ho L. si, Ané C. 2014a. A Linear-Time Algorithm for Gaussian and Non-Gaussian Trait
764 Evolution Models. *Syst Biol.* 63:397–408.
- 765 Ho L.S.T., Ané C. 2014b. Intrinsic inference difficulties for trait evolution with Ornstein-
766 Uhlenbeck models. *Methods in Ecology and Evolution.* 5:1133–1146.
- 767 Howe H.F., Smallwood J. 1982. Ecology of Seed Dispersal. *Annual Review of Ecology and*
768 *Systematics.* 13:201–228.
- 769 Huang G., Jansen H.M., Mandjes M., Spreij P., Turck K.D. 2016. Markov-modulated Ornstein-
770 Uhlenbeck processes. *Advances in Applied Probability.* 48:235–254.
- 771 Ingram T., Mahler D.L. 2013a. SURFACE: detecting convergent evolution from comparative
772 data by fitting Ornstein-Uhlenbeck models with stepwise Akaike Information Criterion.
773 *Methods in ecology and evolution.* 4:416–425.

- 774 Ingram T., Mahler D.L. 2013b. SURFACE: detecting convergent evolution from comparative
775 data by fitting Ornstein-Uhlenbeck models with stepwise Akaike Information Criterion.
776 *Methods in Ecology and Evolution*. 4:416–425.
- 777 Ives A.R., Garland T. 2010. Phylogenetic Logistic Regression for Binary Dependent Variables.
778 *Syst Biol*. 59:9–26.
- 779 Jones C.T., Youssef N., Susko E., Bielawski J.P. 2020. A Phenotype–Genotype Codon Model
780 for Detecting Adaptive Evolution. *Systematic Biology*. 69:722–738.
- 781 Khabbazian M., Kriebel R., Rohe K., Ané C. 2016. Fast and accurate detection of evolutionary
782 shifts in Ornstein–Uhlenbeck models. *Methods in Ecology and Evolution*. 7:811–824.
- 783 Labra A., Pienaar J., Hansen T.F. 2009. Evolution of Thermal Physiology in *Liolaemus* Lizards:
784 Adaptation, Phylogenetic Inertia, and Niche Tracking. *The American Naturalist*.
785 174:204–220.
- 786 Lemey P., Rambaut A., Welch J.J., Suchard M.A. 2010. Phylogeography Takes a Relaxed
787 Random Walk in Continuous Space and Time. *Molecular Biology and Evolution*.
788 27:1877–1885.
- 789 Levin S.A., Muller-Landau *Helene C., Nathan *Ran, Chave *Jérôme. 2003. The Ecology and
790 Evolution of Seed Dispersal: A Theoretical Perspective. *Annual Review of Ecology,*
791 *Evolution, and Systematics*. 34:575–604.
- 792 Lorts C.M., Briggeman T., Sang T. 2008. Evolution of fruit types and seed dispersal:A
793 phylogenetic and ecological snapshot. *Journal of Systematics and Evolution*. 46:396.
- 794 Maddison W.P. 2006. Confounding Asymmetries in Evolutionary Diversification and Character
795 Change. *Evolution*. 60:1743–1746.
- 796 Maddison W.P., FitzJohn R.G. 2015. The Unsolved Challenge to Phylogenetic Correlation Tests
797 for Categorical Characters. *Syst Biol*. 64:127–136.
- 798 Maddison W.P., Midford P.E., Otto S.P., Oakley T. 2007. Estimating a Binary Character’s Effect
799 on Speciation and Extinction. *Syst Biol*. 56:701–710.
- 800 Mahler D.L., Ingram T., Revell L.J., Losos J.B. 2013. Exceptional convergence on the
801 macroevolutionary landscape in island lizard radiations. *Science*. 341:292–295.
- 802 Martin B.S., Bradburd G.S., Harmon L.J., Weber M.G. 2022. Modeling the Evolution of Rates of
803 Continuous Trait Evolution. :2022.03.18.484930.
- 804 May M.R., Moore B.R. 2020. A Bayesian Approach for Inferring the Impact of a Discrete
805 Character on Rates of Continuous-Character Evolution in the Presence of Background-
806 Rate Variation. *Syst Biol*. 69:530–544.
- 807 Middleton N., Thomas D. 1997. *World atlas of desertification.. ed. 2. .*

- 808 Mitov V., Bartoszek K., Stadler T. 2019. Automatic generation of evolutionary hypotheses using
809 mixed Gaussian phylogenetic models. *Proceedings of the National Academy of Sciences*.
810 116:16921–16926.
- 811 Moreno-Jiménez E., Plaza C., Saiz H., Manzano R., Flagmeier M., Maestre F.T. 2019. Aridity
812 and reduced soil micronutrient availability in global drylands. *Nat Sustain*. 2:371–377.
- 813 Nielsen R. 2002. Mapping Mutations on Phylogenies. *Systematic Biology*. 51:729–739.
- 814 Nunes A., Köbel M., Pinho P., Matos P., Bello F. de, Correia O., Branquinho C. 2017. Which
815 plant traits respond to aridity? A critical step to assess functional diversity in
816 Mediterranean drylands. *Agricultural and Forest Meteorology*. 239:176–184.
- 817 O’Meara B. 2008. *Using Trees: Myrmecocystus Phylogeny and Character Evolution and New*
818 *Methods for Investigating Trait Evolution and Species Delimitation (PhD Dissertation)*.
819 *Nat Prec.*:1–1.
- 820 O’Meara, B., & Beaulieu, J. M. (2021, November 6). Potential survival of some, but not all,
821 diversification methods. <https://doi.org/10.32942/osf.io/w5nvd>
- 822 O’Meara B.C., Ané C., Sanderson M.J., Wainwright P.C. 2006. Testing for Different Rates of
823 Continuous Trait Evolution Using Likelihood. *Evolution*. 60:922–933.
- 824 Pagel M. 1994. Detecting correlated evolution on phylogenies: a general method for the
825 comparative analysis of discrete characters. *Proc. R. Soc. B: Biol. Sci.* 255:37–45.
- 826 Pupko T., Pe I., Shamir R., Graur D. 2000. A Fast Algorithm for Joint Reconstruction of
827 Ancestral Amino Acid Sequences. *Mol Biol Evol*. 17:890–896.
- 828 Rabosky D.L., Goldberg E.E. 2015. Model Inadequacy and Mistaken Inferences of Trait-
829 Dependent Speciation. *Syst Biol*. 64:340–355.
- 830 Rao, V., & Teh, Y. W. (2013). Fast MCMC Sampling for Markov Jump Processes and
831 Extensions. *Journal of Machine Learning Research*, 14(11).
- 832 Revell L.J. 2013. A Comment on the Use of Stochastic Character Maps to Estimate Evolutionary
833 Rate Variation in a Continuously Valued Trait. *Systematic Biology*. 62:339–345.
- 834 Revell L.J. 2014. Ancestral Character Estimation Under the Threshold Model from Quantitative
835 Genetics. *Evolution*. 68:743–759.
- 836 Revell L.J. 2021. A variable-rate quantitative trait evolution model using penalized-likelihood.
837 *PeerJ*. 9:e11997.
- 838 Revell L.J., Collar D.C. 2009. Phylogenetic Analysis of the Evolutionary Correlation Using
839 Likelihood. *Evolution*. 63:1090–1100.

- 840 Schupp E.W. 1993. Quantity, quality and the effectiveness of seed dispersal by animals.
841 *Vegetatio*. 107:15–29.
- 842 Schwery O., Onstein R.E., Bouchenak-Khelladi Y., Xing Y., Carter R.J., Linder H.P. 2015. As
843 old as the mountains: the radiations of the Ericaceae. *New Phytologist*. 207:355–367.
- 844 Steel M., Penny D. 2000. Parsimony, Likelihood, and the Role of Models in Molecular
845 Phylogenetics. *Mol Biol Evol*. 17:839–850.
- 846 Stevens P.F., Luteyn J., Oliver E.G.H., Bell T.L., Brown E.A., Crowden R.K., George A.S.,
847 Jordan G.J., Ladd P., Lemson K., Mclean C.B., Menadue Y., Pate J.S., Stace H.M.,
848 Weiller C.M. 2004. Ericaceae. In: Kubitzki K., editor. *Flowering Plants · Dicotyledons:
849 Celastrales, Oxalidales, Rosales, Cornales, Ericales*. Berlin, Heidelberg: Springer. p. 145–
850 194.
- 851 Thomas G.H., Freckleton R.P., Székely T. 2006. Comparative analyses of the influence of
852 developmental mode on phenotypic diversification rates in shorebirds. *Proceedings of the
853 Royal Society B: Biological Sciences*. 273:1619–1624.
- 854 Toljagić O., Voje K.L., Matschiner M., Liow L.H., Hansen T.F. 2018. Millions of Years Behind:
855 Slow Adaptation of Ruminants to Grasslands. *Syst Biol*. 67:145–157.
- 856 Tribble C.M., May M.R., Jackson-Gain A., Zenil-Ferguson R., Specht C.D., Rothfels C.J. 2022.
857 Unearthing modes of climatic adaptation in underground storage organs across Liliales.
858 *bioRxiv*::2021.09.03.458928.
- 859 Uyeda J.C., Harmon L.J. 2014. A novel Bayesian method for inferring and interpreting the
860 dynamics of adaptive landscapes from phylogenetic comparative data. *Systematic
861 biology*. 63:902–918.
- 862 Uyeda J.C., Zenil-Ferguson R., Pennell M.W. 2018. Rethinking phylogenetic comparative
863 methods. *Syst Biol*. 67:1091–1109.
- 864 Vasconcelos, T., Boyko, J. D., & Beaulieu, J. M. (2021). Linking mode of seed dispersal and
865 climatic niche evolution in flowering plants. *Journal of Biogeography*.
- 866 Vasconcelos T., O’Meara B.C., Beaulieu J.M. 2022. A flexible method for estimating tip
867 diversification rates across a range of speciation and extinction scenarios. *Evolution*.
- 868 Venable D.L., Brown J.S. 1988. The Selective Interactions of Dispersal, Dormancy, and Seed
869 Size as Adaptations for Reducing Risk in Variable Environments. *The American
870 Naturalist*. 131:360–384.
- 871 Westoby M., Leishman M., Lord J. 1996. Comparative ecology of seed size and dispersal.
872 *Philosophical Transactions of the Royal Society of London. Series B: Biological
873 Sciences*. 351:1309–1318.
- 874 Yang Z. 2006. *Computational molecular evolution*. Oxford University Press Oxford.

875

876

Supplementary Tables

877 **Table S1.** AIC weights summarizing the average support for each model class when they are the
 878 generating model. Data is generated with $q_{ij} = 0.1$, $\alpha_1 = 3$, $\alpha_2 = 1.5$, $\sigma_1^2 = 0.35$, $\sigma_2^2 = 1$, $\theta_1 =$
 879 2 , and $\theta_2 = 0.75$ for phylogenies with 25, 100, and 250 taxa and model fits using either 25, 100,
 880 or 250 stochastic maps per likelihood iteration. When the generating model class is character
 881 dependent (CD) or character independent (CID+) we expect that the AICwt will be highest for
 882 that model when fit. Character dependent models generally show that pattern, however CID+
 883 models generally perform poorly. An additional concern is datasets simulated by a character
 884 independent model with rate heterogeneity (datasets generated by a CID+ model) are best fit by
 885 CD models – which would be a spurious correlation. Although there was often some signal of
 886 character dependence in these models (AICwt of CD when CID+ is generating), most of the AIC
 887 weight was for simple character independent models (BM1 or OU1).

Generating model class	Generating model type	AICwt of BM1	AICwt of OU1	AICwt of CD	AICwt of CID+	Proportion generating model chosen as best
CD	BMV	0.18	0.17	0.64	0.02	0.62
	OUV	0.03	0.22	0.74	0.02	0.73
	OUA	0.07	0.56	0.31	0.06	0.15
	OUM	0.04	0.02	0.9	0.04	0.92
	OUVA	0.04	0.21	0.7	0.06	0.7
	OUMV	0.02	0.02	0.93	0.03	0.95
	OUMA	0.12	0.15	0.64	0.09	0.66
	OUMVA	0.05	0.13	0.76	0.06	0.76
	OUBM1	0.19	0.58	0.13	0.10	0.08
	OUBMV	0.07	0.20	0.71	0.02	0.73
CID+	BMV	0.36	0.28	0.33	0.03	0.01
	OUV	0.04	0.49	0.43	0.04	0.01
	OUA	0.06	0.56	0.37	0.02	0
	OUM	0.21	0.09	0.03	0.67	0.71
	OUVA	0.07	0.55	0.35	0.04	0.03
	OUMV	0.24	0.19	0.14	0.44	0.44
	OUMA	0.41	0.40	0.13	0.06	0.06
	OUMVA	0.24	0.39	0.21	0.16	0.15
	OUBM1	0.24	0.55	0.16	0.05	0.01
	OUBMV	0.23	0.37	0.30	0.10	0.08

888

889

890

891

892

893

894

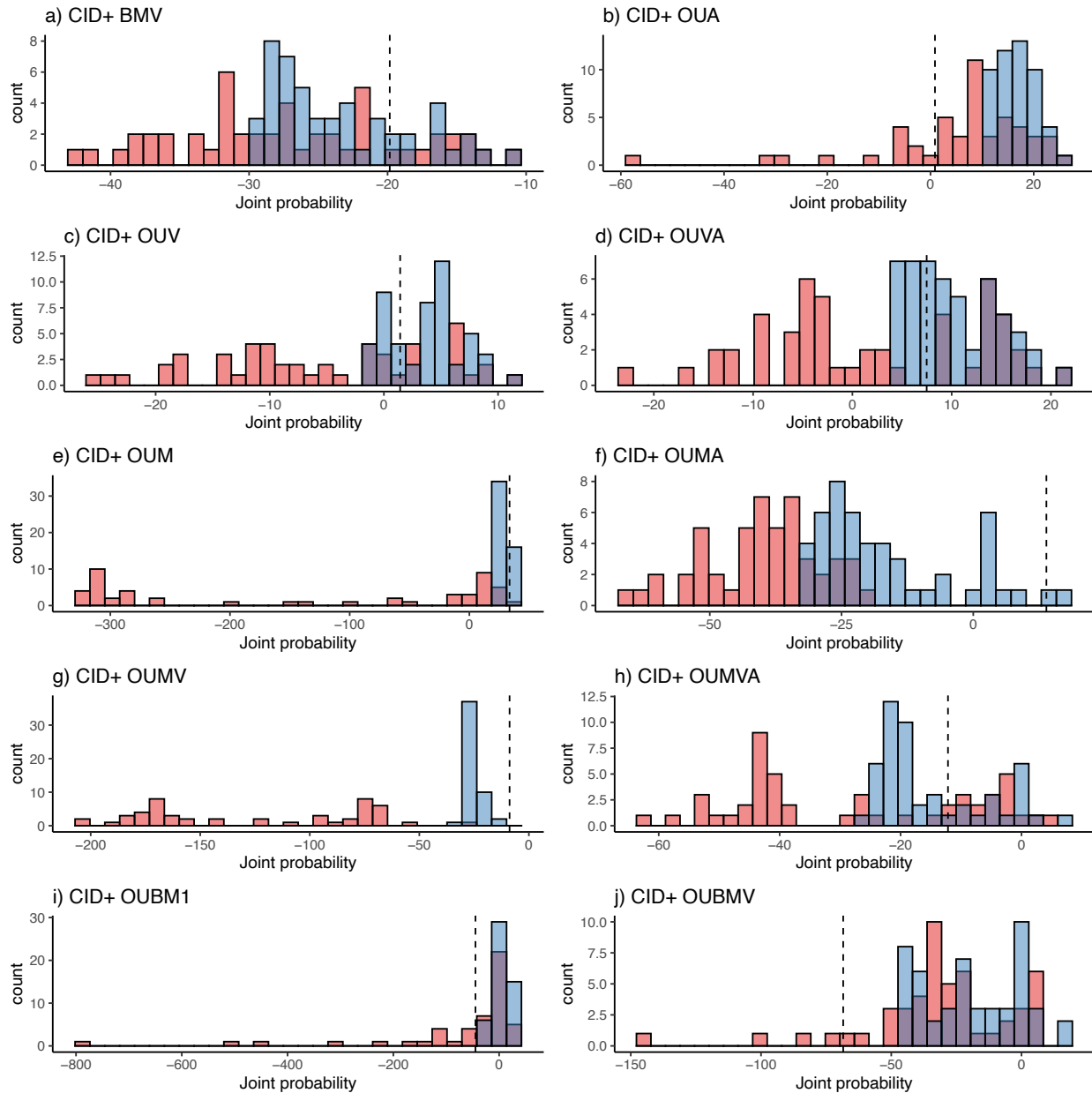
895
 896
 897
 898
 899
 900
 901
 902
 903
 904
 905
 906

Table S2: Modeling results from the 25 models fit to Ericaceae aridity index and fruit type data. Model classes are character independent without rate heterogeneity (CID), character dependence (CD), character independence with rate heterogeneity (CID+), and mixed character dependent and character independence (HYB). Character dependent models suggest that climatic niche evolution will be linked to the fruit type. We found substantial support for OUVA (variable σ^2 and α) and OUMVA (variable σ^2 , α , and θ) models. np is the number of freely estimated parameters. lnLik is the joint likelihood of the MLE. DiscLik and ContLik are the marginal likelihood of the discrete and continuous datasets respectively, given the maximum joint likelihood estimate of the parameters. AIC is the Akaike information criterion, Δ AIC is the difference from the best fit model measured as the difference between each model's AIC, and AICwt is the relative support for each model.

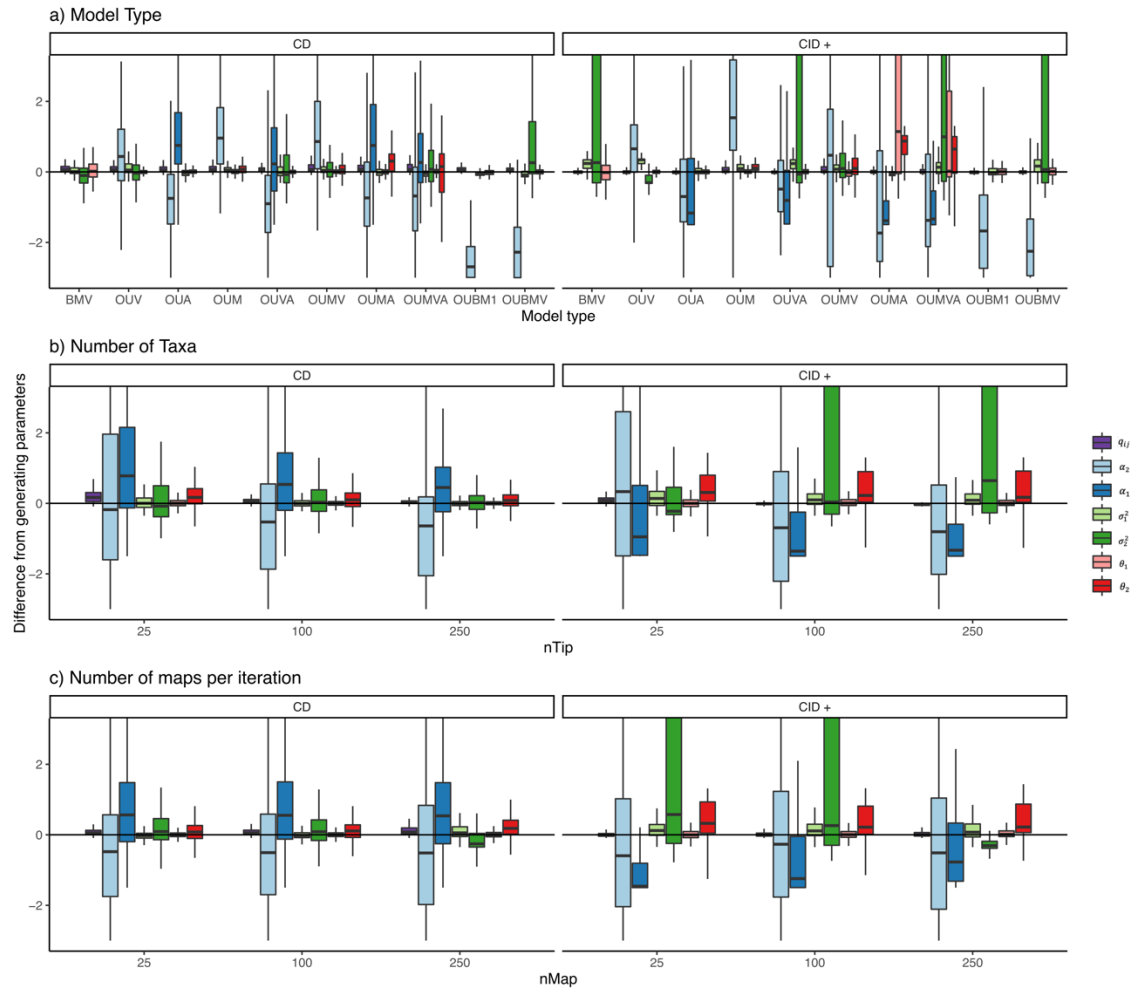
Model class	Model type	np	lnLik	DiscLik	ContLik	AIC	Δ AIC	AICwt
CID	BM1	4	-243.89	-32.62	-206.67	495.78	39.07	0
	OU1	5	-225.5	-32.62	-188.28	461.01	4.30	0.05
CD	BMV	5	-243.78	-32.62	-207.08	497.56	40.85	0
	OUV	6	-225.49	-32.62	-188.47	462.98	6.27	0.02
	OUA	6	-224.95	-32.58	-189.48	461.9	5.19	0.03
	OUM	6	-224.12	-32.57	-187.79	460.24	3.53	0.07
	OUVA	7	-221.62	-32.58	-184.44	457.24	0.53	0.32
	OUMV	7	-224.05	-32.62	-188.15	462.10	5.39	0.03
	OUMA	7	-223.21	-32.58	-187.97	460.42	3.71	0.06
	OUMVA	8	-220.35	-32.60	-183.27	456.71	0	0.41
	OUBM1	5	-243.84	-32.57	-206.67	497.68	40.97	0
	OUBMV	6	-243.79	-32.61	-206.99	499.57	42.87	0
CID+	BMV	7	-244.80	-33.11	-205.78	503.59	46.89	0
	OUV	8	-228.77	-32.98	-190.16	473.55	16.84	0
	OUA	8	-226.42	-33.17	-188.53	468.84	12.13	0
	OUM	8	-226.43	-33.32	-189.07	468.87	12.16	0
	OUVA	9	-244.38	-33.43	-202.12	506.76	50.05	0
	OUMV	9	-225.20	-33.39	-182.88	468.39	11.68	0
	OUMA	9	-225.57	-32.68	-189.92	469.14	12.43	0
	OUMVA	10	-227.39	-33.13	-185.15	474.79	18.08	0
	OUBM1	7	-244.44	-33.16	-206.67	502.88	46.17	0
	OUBMV	8	-225.58	-32.71	-186.58	467.17	10.46	0
HYB	BMS	9	-244.46	-33.08	-204.83	506.93	50.22	0
	OUM	10	-224.12	-32.67	-188.99	468.23	11.52	0
	OUMVA	16	-226.56	-33.03	-179.11	485.13	28.42	0

907

Supplementary Figures

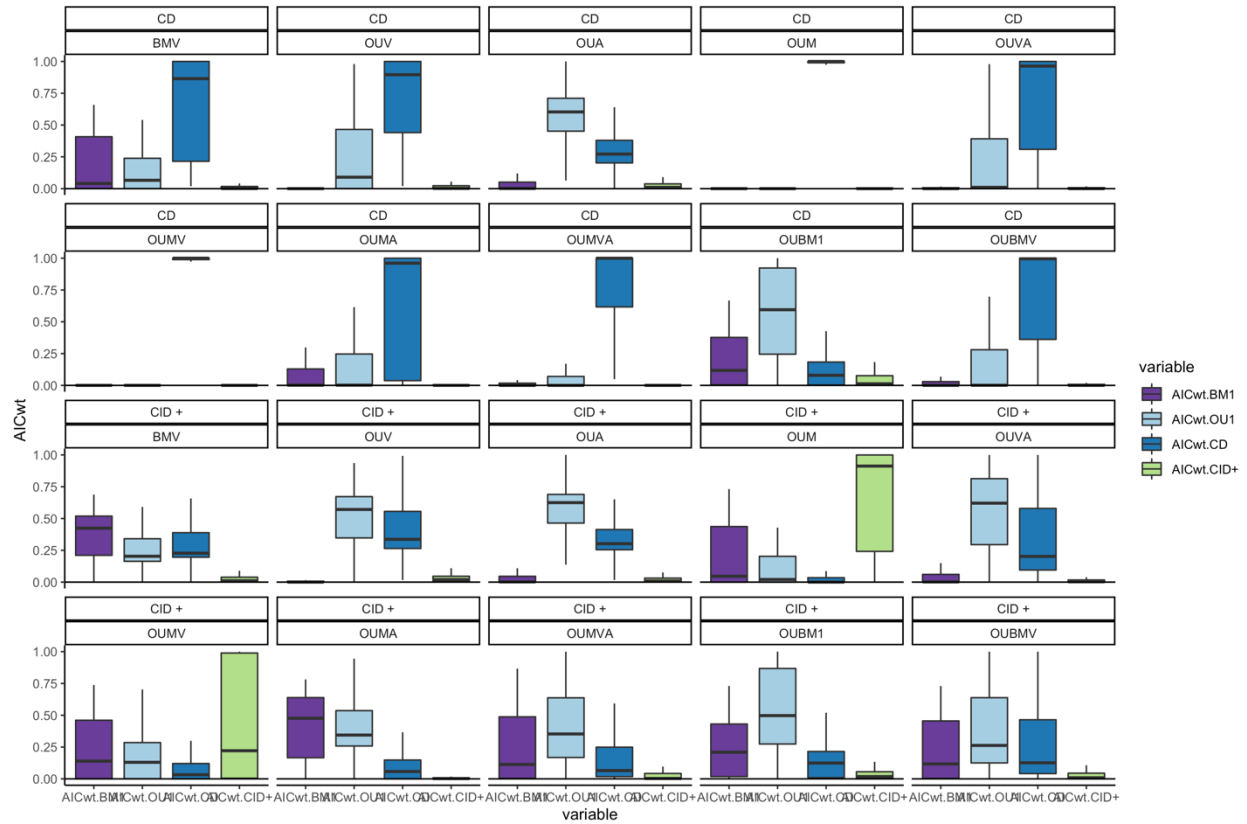


910 **Figure S1.** Overlapping histograms comparing the effectiveness of the adaptive sampling
 911 procedure (blue) and standard discrete only sampling (red) of maps. Regardless of the sampling
 912 procedure, all probabilities are calculated in the same way and so any differences in probabilities
 913 reflects each procedure's ability to generate appropriate mappings. 50 stochastic mappings are
 914 used to calculate the likelihood of the parameters. For each model type, data are simulated
 915 following our methods with $q_{ij} = 0.1$, $\alpha_1 = 3$, $\alpha_2 = 1.5$, $\sigma_1^2 = 0.35$, $\sigma_2^2 = 1$, $\theta_1 = 2$, and $\theta_2 =$
 916 0.75 . Dashed line likelihood under generating map.
 917



918

919 **Figure S2.** The raw difference of the maximum likelihood parameter estimates and the
 920 generating values depending on the a) model type, b) number of taxa in the dataset, and c)
 921 number of stochastic maps per iteration of the likelihood search. Generally, variable alpha
 922 models had the highest biases with alpha being consistently underestimated. As the number of
 923 taxa increased, estimation of CD model parameters was estimated with less error. The number of
 924 maps per iteration had the greatest effect on character independent models with rate
 925 heterogeneity.
 926



927
 928 **Figure S3.** AIC weights summarizing the average support for particular model classes and model
 929 type when they are the generating model. Headings indicate the generating model type and
 930 model class. Data was generated with $q_{ij} = 0.1$, $\alpha_1 = 3$, $\alpha_2 = 1.5$, $\sigma_1^2 = 0.35$, $\sigma_2^2 = 1$, $\theta_1 =$
 931 2 , and $\theta_2 = 0.75$ for phylogenies with 25, 100, and 250 taxa and model fits using either 25, 100,
 932 or 250 stochastic maps per likelihood iteration. When the generating model class is character
 933 dependent (CD) or character independent (CID+) we expect that the AICwt will be highest for
 934 that model when fit.
 935